Available online at www.sciencedirect.com

ScienceDirect

Geochimica et Cosmochimica Acta 177 (2016) 30–47

Geochimica et Cosmochimica Acta

www.elsevier.com/locate/gca

Differences between mono-generic and mixed diatom silicon isotope compositions trace present and past nutrient utilisation off Peru

Kristin Doering [a,b,*], Claudia Ehlert [c], Patricia Grasse [b], Xavier Crosta [d], Sophie Fleury [e], Martin Frank [b], Ralph Schneider [a]

[a] Institute of Geosciences, University of Kiel, Ludewig-Meyn-Str. 10, 24118 Kiel, Germany
[b] GEOMAR Helmholtz Centre for Ocean Research Kiel, Wischhofstr. 1-3, 24148 Kiel, Germany
[c] Max Planck Research Group – Marine Isotope Geochemistry, Carl von Ossietzky University (ICBM), Carl-von Ossietzky-Str. 9-11, 26129 Oldenburg, Germany
[d] UMR CNRS 5805 EPOC – OASU, Université de Bordeaux, Allée Geoffroy Saint Hilaire, 33615 Pessac cedex, France
[e] Hanyang University, 55, Hanyanddaehak-No, Sangnok-Gu, Ansan-si, Gyeonggi-do 15588, South Korea

Received 24 February 2015; accepted in revised form 23 December 2015; Available online 12 January 2016

Abstract

In this study we combine for the first time silicon (Si) isotope compositions of small mixed diatom species ($\delta^{30}Si_{bSiO2}$) and of large handpicked mono-generic (i.e. genus = *Coscinodiscus*) diatom samples ($\delta^{30}Si_{Coscino}$) with diatom assemblages extracted from marine sediments in the Peruvian upwelling region in order to constrain present and past silicate utilisation.

The extension of a previous core-top data set from the Peruvian shelf demonstrates that $\delta^{30}Si_{Coscino}$ values record near-complete Si utilisation, as these are similar to the isotopic composition of the subsurface source waters feeding the upwelling. In contrast, the $\delta^{30}Si_{bSiO2}$ of small mixed diatom species increase southward along the shelf as well as towards the shore. We attribute highest $\delta^{30}Si_{bSiO2}$ values partly to transient iron limitation but primarily to the gradual increase of Si isotope fractionation within the seasonal diatom succession, which are mainly recorded by small diatom species during intense bloom events. In contrast, lower $\delta^{30}Si_{bSiO2}$ values are related to initial Si isotope utilisation during periods of weak upwelling, when low $Si(OH)_4$ concentrations do not permit intense blooms and small diatom species record substantially lower $\delta^{30}Si$ signatures. As such, we propose that the intensity of the upwelling can be deduced from the offset between $\delta^{30}Si_{bSiO2}$ and $\delta^{30}Si_{Coscino}$ ($\Delta^{30}Si_{coscino-bSiO2}$), which is low for strong upwelling conditions and high for prevailing weak upwelling.

We apply the information extracted from surface sediments to generate a record of the present-day main upwelling region covering the past 17,700 years and find that this location has also been characterized by a persistent offset ($\Delta^{30}Si_{coscino-bSiO2}$). By comparison with the diatom assemblages we show that the coastal upwelling system changed markedly between weak and strong upwelling conditions. In addition, our model calculations to quantify species-specific Si isotope fractionation effects based on the diatom assemblages indicate an overall minor influence that cannot explain the high amplitude in the measured $\delta^{30}Si_{bSiO2}$ record.

* Corresponding author at: Institute of Geosciences, University of Kiel, Ludewig-Meyn-Str. 10, 24118 Kiel, Germany. Tel.: +49 431 600 2267.

E-mail addresses: kd@gpi.uni-kiel.de, kdoering@geomar.de (K. Doering).

http://dx.doi.org/10.1016/j.gca.2015.12.029
0016-7037/

1. INTRODUCTION

The silicon (Si) isotope composition ($\delta^{30}Si$) of diatom frustules is used to reconstruct silicic acid ($Si(OH)_4$) utilisation in ocean surface waters in order to better understand the biogeochemical cycling of nutrients and their relationship to the extent of primary productivity (PP). In regions dominated by diatoms, e.g. the Southern Ocean, the North Pacific and coastal upwelling areas, PP is ultimately regulated by $Si(OH)_4$ availability (e.g. Lisitzin, 1971) with large areas of the Southern Ocean also limited by iron availability. Given that diatoms preferentially incorporate the lighter isotopes (^{28}Si and ^{29}Si relative to ^{30}Si) when utilising $Si(OH)_4$ for mineralization of their opaline frustules (De La Rocha et al., 1997), both the residual $Si(OH)_4$ in surface waters and the diatom opal produced from these waters become progressively enriched in the heavier isotopes with increasing $Si(OH)_4$ utilisation (Douthitt, 1982; De La Rocha et al., 1997).

Studies of the modern ocean have contributed to the understanding of the relationship between $\delta^{30}Si$ of biogenic opal ($bSiO_2$) and $Si(OH)_4$ in the context of utilisation, remineralization and dissolution (Varela et al., 2004; Cardinal et al., 2005, 2007; Beucher et al., 2008; Fripiat et al., 2011; Egan et al., 2012; Ehlert et al., 2012; Xiong et al., 2015). These studies are the basis for the use of silicon isotopes from $bSiO_2$ in sediments to reconstruct past changes in $Si(OH)_4$ utilisation (De La Rocha et al., 1998; Beucher et al., 2007; Reynolds et al., 2008; Pichevin et al., 2009; Ellwood et al., 2010; Maier et al., 2013; Ehlert et al., 2013). Core-top calibrations of diatom $\delta^{30}Si$ show that the sedimentary signal reflects the cumulative seasonal drawdown of $Si(OH)_4$ but can be significantly biased by siliceous components other than diatoms (Egan et al., 2012; Ehlert et al., 2012). Moreover, Sutton et al. (2013) reported species-specific Si isotope enrichment factors for several marine diatoms species, which had previously been assumed to be species independent (De La Rocha et al., 1997). Therefore, changes in the dominance of different diatom species on seasonal to geological timescales may substantially influence the reconstructed Si isotope composition of diatom opal in the paleo record and thus the reconstruction of $Si(OH)_4$ utilisation. The potential effects of diatom species-specific Si isotope fractionation thus require a comparison of the $\delta^{30}Si$ signal with shifts in the diatom assemblages in the sedimentary record, in addition to more detailed analyses of modern seasonal variations of the $\delta^{30}Si$ of $Si(OH)_4$ in the surface waters and particulate (diatom) opal in the water column (e.g. Cao et al., 2012).

For the present-day Southern Ocean water column Cardinal et al. (2007) reported Si isotopic signatures of diatoms to be unrelated to particle size (i.e. >0.4 μm, 20–70 μm and >70 μm). This has so far been supported by records of past $\delta^{30}Si$ signatures from the North Pacific (Maier et al., 2013) and Eastern Equatorial Pacific (Ehlert et al., 2013). However, in a case study of the Peruvian coastal upwelling area Ehlert et al. (2012) compared the present-day Si isotope compositions of dissolved $Si(OH)_4$ in the water column ($\delta^{30}Si_{SiOH4}$) with that of diatoms in the underlying surface sediments of the shelf. Their first comparison of Si isotope compositions of mixed diatom species ($\delta^{30}Si_{bSiO2}$; 11–32 μm) and handpicked mono-generic diatoms ($\delta^{30}Si_{Coscino}$; >125 μm; previously reported as $\delta^{30}Si_{diatom}$) revealed $\delta^{30}Si_{bSiO2}$ values being generally lighter than the $\delta^{30}Si_{Coscino}$ values. These lighter $\delta^{30}Si_{bSiO2}$ values may represent low Si utilisation due to continuous upwelling-induced nutrient supply, while $\delta^{30}Si_{Coscino}$ signatures recorded high Si utilisation during non-upwelling or summer conditions.

1.1. Regional setting and present-day upwelling and nutrient conditions off Peru

In the Eastern Equatorial Pacific (EEP) the PP is controlled by the flux of nutrients to the euphotic zone (Barber and Chávez, 1991) transported by year-round upwelling (Pennington et al., 2006). The main source for the upwelled high nutrient waters is the subsurface Peru–Chile Undercurrent (PCUC), which flows southward between 4°S and 14°S at a depth between 50 and 150 m along the shelf (Fig. 1) (Zuta and Guillén, 1970; Brink et al., 1983; Toggweiler et al., 1991). The PCUC is partly fed by eastward flowing subsurface waters of the Equatorial Undercurrent (EUC), the primary Southern Subsurface Counter Current (pSSCC) and secondary Southern Subsurface Counter Current (sSSCC). The ultimate sources of the nutrients are Subantarctic Mode Waters, feeding the EUC (Lukas, 1986) as well as vertical admixture of remineralised organic matter from shelf sediments (Franz et al., 2012; Ehlert et al., 2012).

The high PP associated with high export productivity and remineralisation of organic matter induces an intense Oxygen Minimum Zones (OMZ) (Fuenzalida et al., 2009). Overall the rate of PP is regulated by nutrient supply (macronutrients: nitrate (NO_3^-), $Si(OH)_4$ and phosphate (PO_4); micronutrients: iron (Fe), cadmium), light and physical export (offshore transport or subduction of water masses; Messié and Chavez, 2014). Nutrient concentrations of NO_3^-, PO_4 and partly Fe are very high and thus not limiting for diatom growth off Peru (Bruland et al., 2005; Franz et al., 2012). Instead, $Si(OH)_4$ concentrations are assumed to be limiting diatom production during austral summer (Dugdale et al., 2002; Franz et al., 2012), while Fe and light limitation was shown to prevail during austral winter (Hutchins et al., 2002; Bruland et al., 2005; Pennington et al., 2006; Echevin et al., 2008; Messié and Chavez, 2014). Potential Fe limitation during winter when upwelling is most intense off Peru is in agreement with recent suggestions that Fe limitation can arise in the course of intense upwelling (Pichevin et al., 2014). However, due to the overall high nutrient supply to the near-shore area of the Peruvian coastal upwelling region diatoms are generally the dominant phytoplankton group (Blasco, 1971; Estrada and Blasco, 1985; DiTullio et al., 2005; Bruland et al., 2005; Abrantes et al., 2007).

Diatom assemblages are reliable indicators of the successional stages of PP and record the maturation of upwelling cells in marine sediments (Schuette and Schrader, 1981; MacIsaac et al., 1985; Schrader, 1992; Romero and

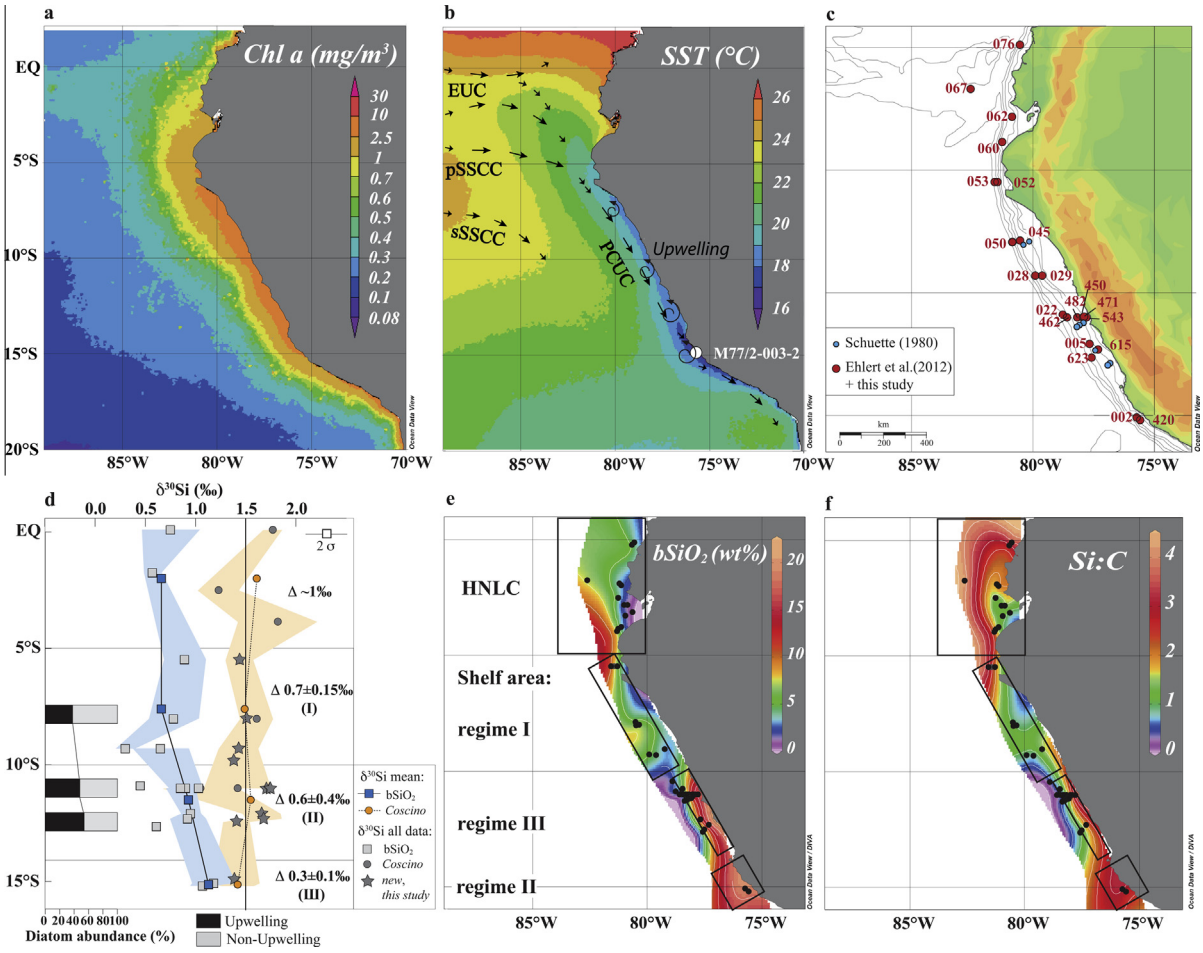

Fig. 1. Maps showing (a) chlorophyll *a* concentration and (b) sea surface temperature averaged for the period between 1997 and 2015 (http://oceancolor.gsfc.nasa.gov/cgi/l3), with generalized circulation pattern of the currents in the near-shore area (modified after Ayón et al., 2008; Montes et al., 2010; Czeschel et al., 2011). EUC Equatorial Undercurrent, pSSCC primary Southern Subsurface Counter Current, sSSCC secondary Subsurface Counter current, PCUC Peru–Chile Undercurrent; The curved arrows near the coast indicate the upwelling of subsurface waters; The location of piston core M77/2-003-2 is given as white circle. (c) Location of surface sediment stations from this study (red circles and labels) and from Schuette (1980) (blue circles); the bathymetry is given for 0–5000 m water depth in 100 m increments; (d) Latitudinal distribution of the surface sediment mean $\delta^{30}Si$ (‰) of $bSiO_2$ (blue squares) and handpicked diatoms (*Coscinodiscus*; orange squares). The $\delta^{30}Si_{bSiO2}$ and $\delta^{30}Si_{Coscino}$ are given as mean values for 0–5°S, 5–10°S, 10–14°S and 15°S (Table 1). The black vertical line at +1.5‰ represents the $\delta^{30}Si_{Si(OH)4}$ value of the source water (PCUC); blue and red shaded areas represent the 2σ error of repeated sample measurements; relative diatom abundances (%) (after Schuette, 1980) for surface sediment indicated by blue circles for the area 5–15°S. The diatom assemblages are classified as upwelling-related (black bars) and non-upwelling diatoms (grey bars); (e) surface sediment $bSiO_2$ concentrations (wt%); (f) surface sediment Si:C ratios; the black rectangles highlight the Northern area and different shelf areas (i.e. regime I, II and III) distinguished accordingly by Chl *a*, SST, $bSiO_2$ and Si:C values (see text for details). (For interpretation of the references to colour in this figure legend, the reader is referred to the web version of this article.)

Hebbeln, 2003). The PP successional stages generally follow four steps (Jones et al., 1983; MacIsaac et al., 1985; Hansen et al., 2014): (1) upwelling of cold, nutrient-rich waters with little biomass and low growth rates, (2) water column stabilisation leads to increase in growth rates and nutrient consumption and diatoms dominate the phytoplankton, (3) due to rapid consumption, nutrient concentrations decrease and higher growth rates result in intense diatom production, and (4) with the onset of nutrient depletion and limitation, growth rates and nutrient uptake diminish. The initial diatom assemblage that occurs during step (2) is composed of small diatoms with high production rates (early diatom succession stage), while the post-upwelling stage (3) is dominated by larger-sized diatoms species (Garrison, 1979; Tarazona et al., 2003). The final stage of nutrient depletion and limitation (4) is usually associated with dinoflagellates and large centric diatoms (Garrison, 1979; Tarazona and Arntz, 2001). Generally the whole cycle is completed in a couple of weeks, but can be interrupted by freshly upwelled water parcels. The change in dominant species is closely related to the transition from turbulent to more stable conditions in upwelled waters (Margalef, 1978; Blasco et al., 1981). Consequently, on an annual basis diatom assemblages follow the same principle of succession

and thus vary depending on the different seasonal environmental conditions (Rojas de Mendiola, 1981; Kemp et al., 2000).

To better understand the factors controlling nutrient utilisation in the course of the PP succession stages using the relationship between $\delta^{30}Si_{bSiO2}$ and $\delta^{30}Si_{Coscino}$, we extended the core-top data set of $\delta^{30}Si_{Coscino}$ from Ehlert et al. (2012) in the main upwelling area off Peru. We further compare the isotopic signatures with the diatom assemblages to evaluate the effect of seasonal and environmental variations, such as upwelling intensity and nutrient availability. The findings from surface sediments are then applied to the $\delta^{30}Si_{bSiO2}$ and $\delta^{30}Si_{Coscino}$ signals as well as the diatom assemblages from a sediment core from the Peruvian upwelling at 15°S covering the last 17,700 years. Additionally, changes in the diatom assemblage will be used to evaluate the influence of species-specific Si isotope fractionation on the Si isotope record.

2. MATERIAL AND METHODS

The data presented in this study were obtained from surface sediments from along the Peruvian shelf and upper slope between 0°N and 15°S (Fig. 1; Table 1) and from latest Pleistocene sediments of piston core M77/2-003-2 (003-2) recovered from 271 m water depth at 15°06′S, 75°41′W (Figs. 1 and 2, Tables 1 and 2). Sediments were retrieved during the German R/V Meteor cruises M77/1 and M77/2 in 2008 in the framework of the Collaborative Research Centre (Sonderforschungsbereich/SFB) 754

Table 1
$bSiO_2$ concentrations and $\delta^{30}Si$ data for mixed diatom species ($\delta^{30}Si_{bSiO2}$) and mono-generic diatoms ($\delta^{30}Si_{Coscino}$) extracted from surface sediments on the Peruvian shelf (modified from Ehlert et al., 2012). 2σ represents the external reproducibility of repeated sample measurements. $\Delta^{30}Si$ corresponds to the difference between $\delta^{30}Si_{Coscino}$ and $\delta^{30}Si_{bSiO2}$. Samples marked in italics are new data presented in this study. The main upwelling area between 5°S and 15°S is divided into three characteristic regimes (I = 5–10°S; II = 10–14°S and III = ~15°S; see text for details) and averaged for $bSiO_2$ concentration, $\delta^{30}Si_{bSiO2}$, $\delta^{30}Si_{Coscino}$ and $\Delta^{30}Si$, as marked in bold. Surface sediment diatom assemblage data are from Schuette (1980). The mean diatom percentages are given for open ocean station and shelf stations (Fig. 1b, blue circles) at 8°S, 11.5°S and 12.5°S. Total Upwell. = cumulative abundance off all upwelling related diatom species in % (*Chaetoceros* spp + *Skeletonema costatum* + *Thalassionema nitzschioides*); Total non-upwell. = 100 − total upwell).

Station no.	Latitude (N)	Longitude (E)	Depth (m)	$bSiO_2$ (wt%)	$\delta^{30}Si$ (‰) $bSiO_2$	2σ	$\delta^{30}Si$ (‰) Coscino	2σ	$\Delta^{30}Si$	1σ
M77/2-076	0.09	−80.56	290	2.8	0.75	0.29	1.77	0.10	1.02	
M77/2-067	−1.75	−82.63	2075	7.1	0.57	0.09	–	–	–	
M77/2-062	−2.5	−81.25	1678	5.1	–	–	1.23	0.21	–	
M77/2-060	−3.85	−81.26	701	4.28			1.82	0.40		
Mean	**0 to −5**		**290–2075**	**4.8**	**0.62**	**0.19**	**1.61**	**0.24**	**1.02**	**–**
M77/2-052	−5.48	−81.45	1252	8.58	–	–	1.44	0.14	–	
M77/2-053	−5.48	−81.57	2607	11.5	0.89	0.21	*1.44*	*0.14*	0.55	
M77/2-045-3	−8	−80.34	359	7.2	–	–	*1.51*	*0.12*	–	
M77/2-050	−8.02	−80.5	1013	7.4	0.78	0.25	1.61	0.17	0.83	
M77/2-028	−9.3	−79.9	1105	5.0	0.30	0.10	–	–	–	
M77/2-029	−9.3	−79.62	437	4.6	0.65	0.28	*1.43*	*0.20*	0.78	
Regime I	**−5 to −10**		**350–2500**	**5–10**	**0.66**	**0.21**	**1.49**	**0.16**	**0.72**	**0.15**
Diatoms groups:		**Upw**	**38%**	**Non-Upw**	**62%**					
M77/2-022	−10.89	−78.77	1923	4.7	0.45	0.25	–	–	–	
M77/1-462	−11	−78.75	2020	5.0	–	–	1.42	0.34	–	
M771-482	−11	−78.24	375	–	–	–	*1.74*	*0.18*	–	
M77/1-450	−11	−78.17	319	13.9	0.90	0.17	*1.74*	*0.12*	0.84	
M771-471	−11	−78.17	316	13.9	–	–	*1.71*	*0.21*	–	
M77/1-469	−11	−77.94	145	17.6	1.03	0.15	1.05	0.38	0.02	
M77/1-543	−11	−77.79	77	12.9	0.85	0.15	–	–	–	
Diatoms groups:		**Upw**	**48%**	**Non-Upw**	**52%**					
M77/1-623	−12.64	−77.58	1085	5.9	0.61	0.13	–	–	–	
M77/1-615	−12.43	−77.41	290	–	–	–	*1.41*	*0.14*	–	
M77/2-005	−12.09	−77.67	214	10.9	0.95	0.10	*1.66*	*0.19*	0.71	
M77/1-620	−12.31	−77.32	150	17.7	0.92	0.18	*1.68*	*0.18*	0.76	
Diatoms groups:		**Upw**	**54%**	**Non-Upw**	**46%**					
Regime II	**−11 to −14**		**50–400**	**10–15**	**0.93**	**0.15**	**1.55**	**0.22**	**0.58**	**0.38**
M77/2-002	−15.08	−75.73	290	20.6	1.18	0.22	*1.41*	*0.24*	0.24	
M77/1-420	−15.19	−75.58	516	17.3	1.07	0.13	*1.42*	*0.16*	0.34	
Regime III	**−15**		**290–516**	**17–20**	**1.1**	**0.18**	**1.4**	**0.20**	**0.29**	**0.07**

funded by the German Science Foundation (DFG). Surface sediment samples were collected with a multicorer (MUC) and only the uppermost cm was used for sample preparation. Particulate organic carbon (C_{org}) and $bSiO_2$ concentrations of the surface sediments were published previously by Mollier-Vogel et al. (2012) and Ehlert et al. (2012) (Supplementary Material, Table S1 and Fig. S1).

Core 003-2 consists of dark olive grey sediments, intercalated with dark greyish to pale yellow laminated intervals. Although smaller slumps and indications of bioturbation can be observed, the sediment record covers the past 17,700 years without major disturbances or hiatuses. The downcore C_{org} concentrations were measured by Mollier-Vogel (2012). The age model, previously established by Mollier-Vogel (2012) was improved by six additional AMS ^{14}C dates measured on the organic fraction soluble in weak sulphuric acid. All measurements were performed at the Leibniz Laboratory for Isotope Research and Dating at the University of Kiel. The 17 AMS ^{14}C results were converted into calendar years using the program CLAM2.2 (Blaauw, 2010), the Marine13 calibration curve (Reimer and Bard, 2013) and applying a reservoir age of 511 ± 278 years following Ortlieb et al. (2011) (Supplementary Material, Table S2). The program CLAM2.2 (Blaauw, 2010) is based on a Bayesian method and was used in order to provide the best fit between radiocarbon ages. The resulting age model is displayed in Fig. S2 of the Supplementary Material.

2.1. Diatom assemblages

Sediment treatment and slide preparation for the analyses of diatom assemblages from Core 003-2 followed the technique described by Rathburn et al. (1997). Diatom counting followed the procedures described by Crosta and Koç (2007). An average of 350 diatom valves were counted per sample at ×1000 magnification and the total number of diatom valves per gram of dry sediment was calculated as follows:

$$Valves/g = ((N/n) \times (S/s) \times (V/v))/W,$$

where N is the number of valves counted and n the number of fields of view, S is the area of the evaporation tray, s the area of one field of view, V the volume of solution in the beaker, v the volume of solution put in the evaporation tray and W the weight of the sample. Total diatom numbers are presented in units of 10^6 valves per gram dry sediment (Supplementary Material, Table S3; after Schrader and Gersonde, 1978). Additionally, to provide an estimate of the composition of the 11–32 µm fraction, smear-slides were prepared and counted at 400× magnification.

The abundances of two groups of diatom species representing upwelling and non-upwelling conditions were identified according to earlier studies off Peru (Schuette, 1980; De Vries and Schrader, 1981; Rojas de Mendiola, 1981; Schuette and Schrader, 1981; Abrantes et al., 2007).

(1) *Coastal upwelling – nutrient-rich, turbulent waters (initial diatom succession stage, step 2): Chaetoceros* spp. and resting spores (RS), *Skeletonema costatum*, *Thalassionema nitzschioides* var. *nitzschioides*; *Chaetoceros* spp. is the most dominant species and forms of resting spores (RS) when nutrients are nearly exhausted in the euphotic zone (Schuette, 1980). *Thalassionema nitzschioides* and *Skeletonema costatum* are mainly associated with high nutrient conditions or freshly upwelled waters (Blasco, 1971; Margalef, 1978 Romero and Hebbeln, 2003).

(2) *Non-upwelling diatom species:*
Coastal planktonic (temperate, cosmopolitan) – high-to-moderate nutrient waters (PP cycle, step 3): *Actinocylcus* spp., *Actinoptychus* spp., *Asteromphalus* spp., *Coscinodiscus* spp.; Coastal planktonic species are generally found in the water and sediments close to the coast, their spatial distribution pattern resembles that of upwelling group (1) (Schuette, 1980; Romero and Hebbeln, 2003) but they are associated with high to moderate surface water productivity and non turbulent conditions (Blasco, 1971; Rojas de Mendiola, 1981; Romero et al., 2003; Romero and Hebbeln, 2003).
Oceanic planktonic (warm, temperate) in nutrient-poor waters (PP cycle, step 4): *Azpeitia* spp., *Nitzschia* spp., *Rhizosolenia* spp., *Thalassiosira* spp.; Oceanic planktonic diatoms are often referred to as the tropical/subtropical group associated with low- to mid-latitude pelagic warm waters (Romero and Hebbeln, 2003).
Other diatom species: *Cyclotella* spp., (mainly *C. striata* and *C. stylorum*), *Biddulphia* spp. (mainly alternans), *Cocconeis* spp., *Delphineis karstenii*; Planktonic and benthic marine to brackish species thriving in littoral environments indicating transport from the coast to the core site.

For simplification species overall accounting for less than 2% are not shown here but a complete overview is given in Supplementary Material (Table S3). Handpicked diatoms were identified at 200–1000× magnification at irregular intervals and belong mainly to *Coscinodiscus asteromphalus*, *C. radiatus* and *C. concinnus* as part of group 2 (coastal planktonic diatoms).

2.2. Biogenic opal and silicon isotope analyses

The $bSiO_2$ concentration of the sediments, which represents the relative contribution of opal producing organisms (mainly diatoms, but also radiolarians and sponge spicules), was quantified according to an automated leaching method using sodium hydroxide (DeMaster, 1981; Müller and Schneider, 1993) at a precision of 1–2% (1σ) (Tables 1 and 2). For the downcore record of core 003-2 the $bSiO_2$ accumulation rates (AR_{bSiO2} g cm^{-2} ka^{-1}; Table 2) were calculated using the dry bulk density (g/cm^3) and the sedimentation rates (cm/ka) obtained based on the age model.

Diatoms were extracted from the sediment for the silicon isotope measurements in two different ways. For the $\delta^{30}Si_{bSiO2}$ measurements the size fraction 11–32 µm was separated using chemical and physical cleaning techniques

(sieving and heavy liquid separation) as described by Morley (2004). Following Morley et al. (2004) the 11 μm grain size was used as lower size limit to completely remove clay minerals, while the 32 μm size fraction was selected as the upper grain size limit to remove the generally larger radiolarians, as well as sponge spicules. All samples were scanned via light microscopy to verify their purity with respect to the detrital (clay) fraction and other opal phases prior to dissolution until pure (>95%) diatom samples were obtained. According to smear slide counts radiolarian and sponge spicules accounted for less than 1% and 5%, respectively (Supplementary Material, Fig. S3). In an additional procedure 200–500 large centric diatoms (*Coscinodiscus* spp.) were handpicked from the 125/150–250 μm size fraction to analyse the $\delta^{30}Si_{Coscino}$ signatures (after Ehlert et al., 2012).

From all samples an aliquot (~75 μL) was transferred into Teflon vials and dissolved in 1 mL 0.1 M NaOH at 130 °C over 12 h. Residual material was separated via centrifugation and remaining organic matter was removed by adding 200 μL concentrated H_2O_2 (Suprapur). Sample solutions were diluted with 4 mL MilliQ water and neutralised with 0.1 mL 1 M HCl (Reynolds et al., 2008). Al/Si ratios were measured on aliquots of the dissolved $bSiO_2$ samples using an *Agilent 7500 Series* quadrupole ICPMS at GEOMAR, Kiel to check for potential remaining contamination by clays (Table 2) and ranged between 2 and 210 mmol/mol (for the evaluation see Supplementary Material S3). Silicate concentrations of all sample solutions were measured colourimetrically using a photospectrometer (Grasshoff et al., 1999) and chromatographically purified on columns containing 1 mL pre-cleaned AG50W-X8 cation exchange resin (BioRad, mesh 200–400) following the method described by Georg et al. (2006) and modified by de Souza et al. (2012).

Silicon isotope ratios were determined on a *NuPlasma HR* Multi Collector-ICPMS at GEOMAR applying a standard-sample bracketing method (Albarède et al., 2004). Sample solutions were diluted to a Si concentration of 0.6 ppm and introduced into the MC-ICPMS via a Cetac Aridus II desolvating nebulizer system equipped with a PFA nebulizer with a 60–80 μL/min uptake rate. Silicon isotope compositions are reported in δ-notation against the reference standard NBS28 in parts per thousand ($\delta^{30}Si = ((R_{sample}/R_{standard}) - 1) * 1000$), where R is the measured $^{30}Si/^{28}Si$ ratio of the sample and the NBS28 standard, respectively. All samples were measured on at least three different days and at least 4–5 times per session, which resulted in uncertainties between 0.06‰ and 0.31‰. This external reproducibility is given as 2σ standard deviations of the mean $\delta^{30}Si$ value (Tables 1 and 2). Long-term repeated measurements of the reference materials NBS28, IRMM018, and Big Batch gave average $\delta^{30}Si$ values of 0.00 ± 0.23‰ (2σ), -1.51 ± 0.18‰ (2σ) and -10.74 ± 0.20‰ (2σ), respectively, which agree well with reported literature values (Reynolds et al., 2007). Overall, external reproducibility was within the long-term precision of ±0.23‰ (2σ). The latter is indicated by an error bar on all figures, while the external reproducibility of the samples is indicated by coloured areas.

3. RESULTS

3.1. Surface sediment stable silicon isotope compositions, Si:C ratios and diatom assemblages

The surface sediment data set in this paper comprises the previous study of Ehlert et al. (2012) and eleven new Si isotope measurements of handpicked diatoms ($\delta^{30}Si_{Coscino}$) from the main upwelling area (see Table 1; Fig. 1d). The $\delta^{30}Si_{bSiO2}$ signatures are highly variable and increase from +0.6‰ to +1.1‰ in the South and decreases from the coast (+1‰) to lower values further offshore (+0.3‰; Table 1). In contrast, the $\delta^{30}Si_{Coscino}$ values are usually higher and exhibit little variability ($+1.5 \pm 0.3$‰) with one exception at 11°S where a low value of $+1 \pm 0.38$‰ was found. However, even this low $\delta^{30}Si_{Coscino}$ value is still within the uncertainty of the mean value. The offset between $\delta^{30}Si_{Coscino}$ and $\delta^{30}Si_{bSiO2}$ signatures ($\Delta^{30}Si_{coscino-bSiO2} = \delta^{30}Si_{Coscino} - \delta^{30}Si_{bSiO2}$) is highest in the North (0–5°S; $\Delta^{30}Si_{coscino-bSiO2} = 1$‰) and considerably lower within the main upwelling area (5–10°S: $\Delta^{30}Si_{coscino-bSiO2} = 0.7 \pm 0.15$‰; 10–14°S: $\Delta^{30}Si_{coscino-bSiO2} = 0.6 \pm 0.4$‰; 15°S: $\Delta^{30}Si_{coscino-bSiO2} = 0.3 \pm 0.1$‰) (All $\Delta^{30}Si_{coscino-bSiO2}$ values reported are positive, and for better distinction from $\delta^{30}Si$ signatures we omit a prefix; Table 1; Fig. 1d). Additionally, at 11°S and 12°S $\delta^{30}Si_{bSiO2}$ values decrease from the coast to the shelf-break indicating the influence of dynamic coastal processes. To focus on the high productivity near-shore process the regionally averaged $\Delta^{30}Si_{coscino-bSiO2}$ value (0.6 ± 0.4‰) between 10°S and 14°S (regime II) was calculated only for the samples from depths shallower than 500 m (i.e. excluding station 22 and 623; Supplementary Material, Fig. S4).

The differences in the $bSiO_2$ and C_{org} distributions (previously presented by Ehlert et al., 2012 and Mollier-Vogel et al., 2012) result in higher Si:C ratios (>3) at offshore locations in the North (0–5°S) and close to the coast in the South (10–15°S), while on the central shelf (5–10°S) the Si:C ratios remain close to 1 (Fig. 1f).

Due to lack of counts of the diatom assemblage from the core-top material presented here, assemblage data are used from Schuette, 1980 (Fig. 1c and d). The diatom assemblages on the shelf show a slight increase in the contributions of upwelling-related over non-upwelling species from North (38% upwell/62% non-upwell) to South (54% upwell/46% non-upwell; Table 1 and Fig. 1d).

3.2. Downcore diatom assemblages, silicon isotope compositions and accumulation rates of $bSiO_2$ and C_{org}

The diatom assemblage record of core 003-2 shows variations in the amount of upwelling-related and non-upwelling diatom groups from the deglaciation to the Holocene (Table 3; Fig. 2a and b), while the total diatom abundance (Fig. 2g) closely follows the maximum percentages of upwelling-related diatom species. However, based on estimates of smear-slides performed on core 003-2 the 11–32 μm size fraction samples did not contain diatom species smaller than 11 μm such as *S. costatum*, *T. nitzschioides*

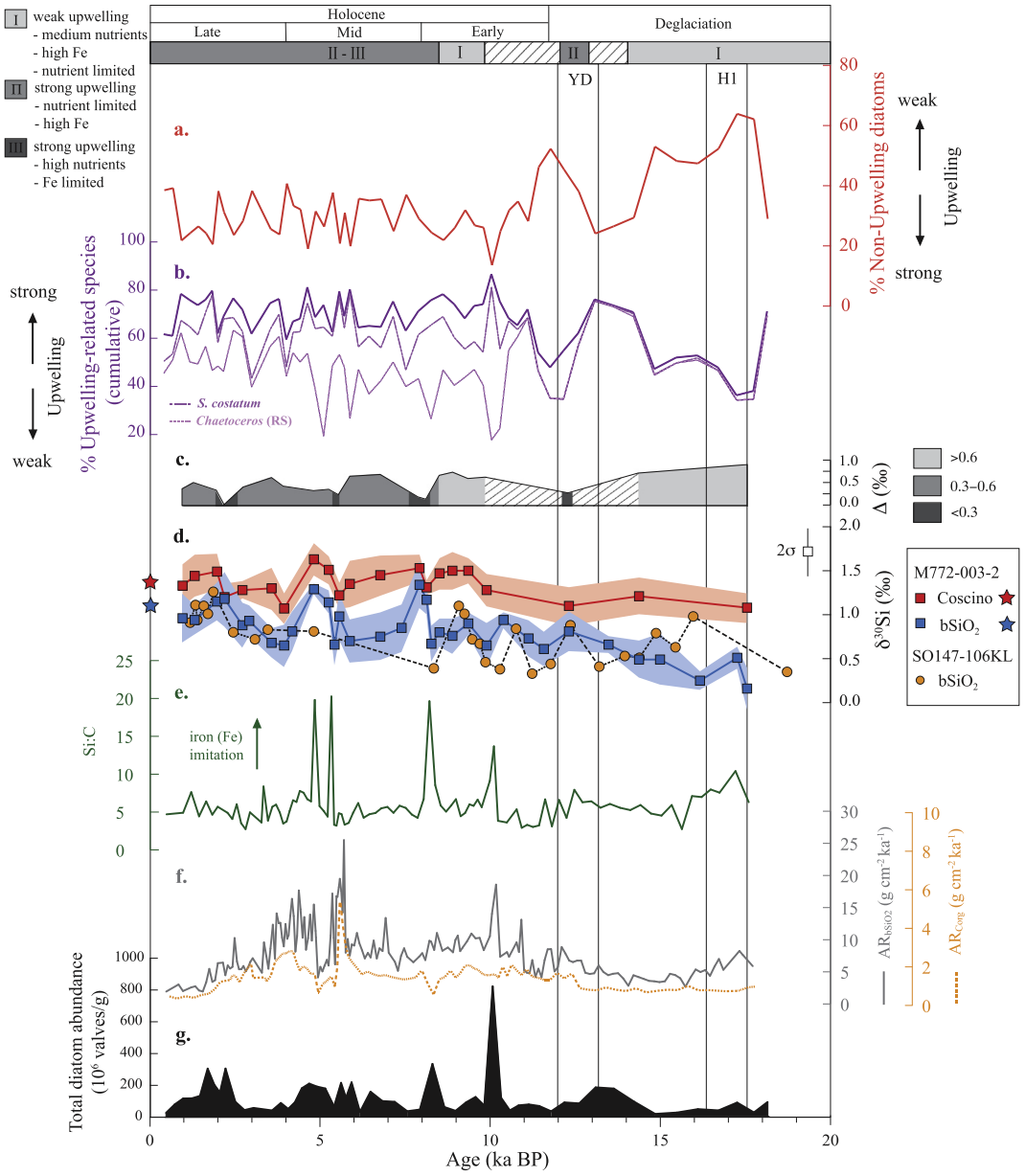

Fig. 2. Downcore records from core M77/2-003-2; Percentages of (a) non-upwelling-related diatom species (red line) and (b) upwelling-related diatom species (purple line), within (b) cumulative contribution of *Chaetoceros* (RS; light purple dotted line) and *S. costatum* (purple dashed line) are shown; (c) Δ ($\Delta^{30}Si_{coscino-bSiO2}$) (grey shadings indicate the different regimes, see legend); (d) $\delta^{30}Si_{bSiO2}$ (blue squares) and $\delta^{30}Si_{Coscino}$ (red squares) as well as the $\delta^{30}Si_{bSiO2}$ record of core SO147-106KL from 12°S (orange circles; Ehlert et al., 2013); blue and red shaded areas represent 2σ error of repeated sample measurements; the blue and red stars mark the core-top values of both fractions of core M77/2-002 (Ehlert et al., 2012). (e) Si:C ratios; (f) AR_{bSiO2} (g cm^{-2} ka^{-1}; solid grey line) and AR_{Corg} (g cm^{-2} ka^{-1}; orange dotted line); (g) total diatom abundance of core (# 10^6 valves/g of dry sediment; black area); Time periods are classified as: (I) weak upwelling based on lowest diatom valve abundance (<50 × 10^6 valves/g) and decreased percentages of upwelling-related diatom species (<70%) but higher Si:C ratios of 5–10 indicative of increased iron limitation (II) stronger upwelling based on elevate diatom abundance between 50 and 200 × 10^6 valves/g, a high percentage of upwelling-related species (>70%) but lower Si:C ratios (~5) indicating reduced iron limitation; (III) strong upwelling based on highest diatom abundance (>200 × 10^6 valves/g), diatom assemblages dominated by upwelling-species (>70%) and high Si:C ratio (5–20) indicating iron limitation. (For interpretation of the references to colour in this figure legend, the reader is referred to the web version of this article.)

or vegetative cells of *Chaetoceros* spp. due to the sample processing (e.g. sieving and gentle ultrasonication). This results in overall lower abundances of upwelling species (*Chaetoceros* RS) between 5% and 25% with only 5–10% during the deglaciation and up to 25% during the Holocene at 11 ka, 6 ka and 2 ka BP (Supplementary Material, Fig. S5). The total diatom abundance remains generally low (20–100 × 10^6 valves/g) during the deglaciation but shows a broad peak centred around 13 ka (~200 × 10^6 valves/g). During the Early (11.7–8.2 ka BP)

Table 2
Downcore records for AR_{bSiO2} values (g cm^{-2} ka^{-1}), Si:C ratios, δ^{30}Si (mixed species and handpicked diatoms) and Al/Si elemental ratios obtained from core M77/2-003-2 and resulting Δ^{30}Si values; 2σ represents the external reproducibility of repeated sample measurements.

Age (ka)	AR_{bSiO2} (g/cm^3/kyr)	Si:C	δ^{30}Si (‰) $bSiO_2$	2 σ	Al/Si (mmol/mol)	δ^{30}Si (‰) Coscino	2σ	Δ^{30}Si	Regime (I, II or III)
0.95	2.01	4.91	0.96	0.27	30	1.33	0.24	0.37	III
1.31	2.75	–	0.94	0.16	6	1.44	0.23	0.40	III
1.97	6.35	5.70	1.15	0.21	20	1.49	0.20	0.34	III
2.19	4.47	–	1.18	0.31	2	1.20	0.16	0.02	III
2.72	5.91	–	0.88	0.25	36	1.28	0.09	0.41	II
2.92	6.55	4.96	0.93	0.17	6	–	–		II
3.58	12.34	5.70	0.68	0.16	8	1.30	0.24	0.62	II
3.95	12.46	–	0.65	0.24	12	1.07	0.17	0.43	II
4.19	13.68	6.56	0.81	0.22	29	–	–		III
4.83	11.38	19.81	1.29	0.06	7	1.63	0.18	0.33	III
5.27	10.64	–	1.14	0.13	15	1.51	0.15	0.36	III
5.44	16.77	–	0.66	0.23	23	–	–		II
5.58	17.58	–	0.98	0.26	7	1.22	0.15	0.24	III
5.89	9.27	–	0.70	0.24	27	1.35	0.26	0.62	II
6.79	8.23	5.49	0.75	0.26	6	1.45	0.22	0.70	II
7.42	8.67	–	0.85	0.27	12	–	–		II
7.95	7.91	–	1.34	0.26		1.53	0.15	0.19	III
8.16	9.84	–	1.17	0.16	4	1.31	0.08	0.14	III
8.30	8.40	–	0.67	0.20	8	–	–		II
8.54	8.28	5.86	0.80	0.15	35	1.47	0.18		II
8.92	9.96	–	0.76	0.20	6	1.50	0.21	0.47	II
9.39	10.96	6.02	0.90	0.12	18	1.50	0.14	0.60	II
9.93	10.55	–	0.65	0.25	55	1.28	0.18	0.75	II
10.43	8.07	–	0.94	0.08	9	–	–		II
11.17	6.83	–	0.73	0.20		–	–		I
11.62	8.51	6.68	0.61	0.19	22	–	–	–	I
12.36	6.52	–	0.81	0.22	12	1.10	0.21	0.28	III
13.53	4.70	6.07	0.66	0.09	–	–	–		I
14.43	3.90	5.93	0.49	0.21	81	1.21	0.20	0.72	I
15.05	3.53	4.53	0.49	0.28	17	–	–		I
16.23	5.28	6.98	0.25	0.10		–	–		I
17.33	7.63	–	0.51	0.12	28	–	–		I
17.62	5.89	6.30	0.16	0.23	209	1.08	0.16	0.91	I

and Mid Holocene (8.2–4 ka BP) non-upwelling species were less abundant, accounting for less than 40% of the overall diatom assemblage, while the contribution of the upwelling-related species increased (60–80%). Overall four periods of highest contributions of upwelling-related diatoms and total diatom abundances occurred during the Holocene at 9.7 ka, 7.9 ka, 5.7–4.3 ka and 2–1.3 ka (Fig. 2b).

During the deglaciation (17.7–11.7 ka BP) the AR_{bSiO2} and AR_{Corg} are around 5 ± 1.5 and 0.9 ± 0.3 g cm^{-2} ka^{-1}, while the Si:C ratios are on average as high as 6 ± 1.7. The low mean $\delta^{30}Si_{bSiO2}$ (+0.5 ± 0.4‰) and $\delta^{30}Si_{Coscino}$ (+1.1 ± 0.15‰) signatures during the deglaciation result in high $\Delta^{30}Si_{coscino-bSiO2}$ values around 0.8 ± 0.1‰, with the exception of a low signature of 0.3‰ during the Younger Dryas (YD; 12.8–11.7 ka BP) (Fig. 2c; Table 2).

During the Holocene the AR_{bSiO2} increased to 9 ± 4 (g cm^{-2} ka^{-1}) with maximum values at 10 ka, 5.3 ka and 4.8 ka BP. Similarly, AR_{Corg} values increase to 1.7 ± 0.8 g cm^{-2} ka^{-1} and maximum values of 5 g cm^{-2} ka^{-1} at 5.5 ka and 3 at 4 ka BP. The Si:C ratios are on average at 6 ± 3.6 and exhibit distinct maxima of up to 20 at 10 ka, 8.2 ka, 5.3 ka and 4.8 ka BP. During the Holocene $\delta^{30}Si_{bSiO2}$ and $\delta^{30}Si_{Coscino}$ signatures increase to overall higher mean values (+0.9 ± 0.4‰ and +1.4 ± 0.3‰). The $\delta^{30}Si_{bSiO2}$ record shows little variability between 11 ka and 8 ka BP (+0.8 ± 0.1‰), followed by a peak of +1.3‰ that slightly lags behind the maximum observed in AR_{bSiO2}, Si:C and diatom abundance. The $\delta^{30}Si_{Coscino}$ signatures increase to +1.4 ± 0.1‰ between 10 ka and 6 ka BP with only a slight decrease at 8 ka BP. Accordingly, the $\Delta^{30}Si_{coscino-bSiO2}$ values remain high at 0.7 ± 0.1‰ until 8.2 ka and decrease considerably afterwards to +0.2 ± 0.03‰ at the transition from the Early to the Mid Holocene (8 ka BP) while remaining above 0.6‰ during the Mid and Late (4–0 ka BP) Holocene. During the Mid and Late Holocene (8–6 ka BP and 4.2–2.2 ka BP) both $\delta^{30}Si_{bSiO2}$ and $\delta^{30}Si_{Coscino}$ decrease to +0.8 ± 0.21‰ and +1.3 ± 0.16‰, interrupted by maximum values of +1.2 ± 0.1‰ and +1.5 ± 0.1‰, at 8 ka, 5.3–4.2 ka and 2.2–1.8 ka BP, respectively. Correspondingly, the $\Delta^{30}Si_{coscino-bSiO2}$ values are low (0.25 ± 0.15‰) during prevailing maximum $\delta^{30}Si_{bSiO2}$ signatures (+1.2 ± 0.1‰), but higher (0.5 ± 0.19‰) during periods when $\delta^{30}Si_{bSiO2}$ decreases (+0.8 ± 0.21‰).

Table 3
Downcore abundance of diatom species and groups over time for core M77/2-003-2 as well as the calculated values for ε_{ass}. ε_{ass} (marked in bold) was calculated using the abundance of Upwelling (1) and Non-Upwelling (2) diatom groups (%) (marked in bold) based on eq. (1; see discussion chapter 4.3 for details). *Chaet.* = *Chaetoceros* spp.; *Skel.* = *Skeletonema costatum*; *O–C* = *Others* (%)–*Chaetoceros* spp. (%); Total upwell. = The cumulative abundance off all upwelling related diatom species in%; Non-Upwelling = 100% − Total Upwell (%).

Age (ka)	Abundance Valves × 10^6	Chaet (%)	Skel. (%)	O–C (%)	ε_{ass}	Upwell (%)	Non-Upwell (%)
0.38	24	45	5	55	**−1.55**	**61**	**39**
0.63	77	51	3	49	**−1.60**	**61**	**39**
0.87	114	62	5	38	**−1.71**	**78**	**22**
1.12	115	50	15	50	**−1.59**	**76**	**24**
1.35	131	49	12	51	**−1.59**	**74**	**26**
1.57	303	56	14	44	**−1.66**	**76**	**24**
1.76	201	46	31	54	**−1.56**	**80**	**20**
1.92	152	48	10	52	**−1.58**	**62**	**38**
2.08	303	46	22	54	**−1.56**	**69**	**31**
2.36	94	63	5	37	**−1.72**	**76**	**24**
2.62	42	60	2	40	**−1.70**	**72**	**28**
2.88	55	40	4	60	**−1.49**	**62**	**38**
3.41	39	56	7	44	**−1.66**	**74**	**26**
3.66	86	60	9	40	**−1.70**	**76**	**24**
3.87	49	44	4	56	**−1.54**	**59**	**41**
4.06	91	54	9	46	**−1.63**	**67**	**33**
4.26	179	50	13	50	**−1.59**	**68**	**32**
4.47	208	53	21	47	**−1.63**	**81**	**19**
4.69	189	38	25	62	**−1.48**	**69**	**31**
4.93	177	19	45	81	**−1.29**	**74**	**26**
5.18	65	48	12	52	**−1.58**	**62**	**38**
5.38	213	53	24	47	**−1.62**	**79**	**21**
5.52	119	48	16	52	**−1.57**	**69**	**31**
5.68	216	27	52	73	**−1.36**	**80**	**20**
5.92	30	47	9	53	**−1.56**	**64**	**36**
6.22	157	37	24	63	**−1.46**	**65**	**35**
6.56	98	42	14	58	**−1.52**	**64**	**36**
6.91	94	50	19	50	**−1.59**	**75**	**25**
7.27	34	40	7	60	**−1.49**	**63**	**37**
7.63	45	43	18	57	**−1.53**	**71**	**29**
7.99	332	26	39	74	**−1.36**	**76**	**24**
8.33	61	47	22	53	**−1.56**	**78**	**22**
8.65	37	40	20	60	**−1.50**	**74**	**26**
8.95	90	43	12	57	**−1.53**	**68**	**32**
9.22	124	47	12	53	**−1.56**	**73**	**27**
9.47	70	40	14	60	**−1.50**	**74**	**26**
9.71	821	18	64	82	**−1.27**	**86**	**14**
9.95	119	22	33	78	**−1.32**	**75**	**25**
10.20	40	55	12	45	**−1.64**	**68**	**32**
10.45	71	60	3	40	**−1.70**	**65**	**35**
10.74	77	68	0	32	**−1.78**	**72**	**28**
11.04	67	46	0	54	**−1.56**	**54**	**46**
11.38	34	35	0	65	**−1.44**	**48**	**52**
11–76	90	34	0.3	66	**−1.44**	**55**	**45**
12.18	83	56	0.7	44	**−1.66**	**62**	**38**
12.65	184	75	0.0	25	**−1.84**	**76**	**24**
13.17	177	73	0.3	27	**−1.82**	**73**	**27**
13.75	94	69	1	31	**−1.78**	**71**	**29**
14.35	17	44	0.4	56	**−1.54**	**47**	**53**
14.97	26	50	0	50	**−1.59**	**52**	**48**
15.57	47	51	1	49	**−1.60**	**53**	**47**
16.16	40	46	0	54	**−1.56**	**48**	**52**
16.69	89	34	0	66	**−1.44**	**36**	**64**
17.17	27	34	0	66	**−1.44**	**38**	**62**
17.56	92	69	0	31	**−1.79**	**71**	**29**

4. DISCUSSION

4.1. Differences in biogeochemical regimes along the modern shelf

The characteristic year-round upwelling and high PP off Peru (Pennington et al., 2006) are generally contrasted by low PP at open-ocean areas further offshore and in the equatorial upwelling region in the North. The latter regions receive significantly less nutrients due to absent or weaker upwelling of subsurface waters and are generally limited in Fe due to low contributions from atmospheric dust. As such, the open ocean and the equatorial upwelling systems are described as High-Nitrate-Low-Chlorophyll (HNLC) areas, where PP is thought to be co-limited by $Si(OH)_4$ and Fe supply (Dugdale et al., 1995; Hutchins et al., 2002). Overall, the differences in upwelling intensity and PP between the shelf and these HNLC areas is indicated by the distribution of annually averaged Chlorophyll a concentrations and Sea Surface Temperatures (Fig. 1a and b). Furthermore, along the shelf upwelling intensity increases from North to South (SST decreases, respectively) and PP is highest within 100 km from the coast (highest Chl *a*). Over the shelf PP is generally not limited by Fe, which is released under oxygen-deficient bottom-water conditions from upper shelf sediments (<600 m; Hutchins and Bruland, 1998; Johnson et al., 1999; Bruland et al., 2005; Noffke et al., 2012) and upwelled waters become enriched in iron through interaction with bottom sediments. Therefore, the shelf width has a major influence on iron supply with higher Fe concentrations supplied from a wider shelf and lower concentrations where the shelf is narrow (Johnson et al., 1999; Bruland et al., 2005). However, it has to be noted that sulphidic conditions at the shallow shelf can lead to a retention of iron in the sediments (Scholz et al., 2014).

Overall, we assume that Fe supply is high above the wide central Peruvian shelf (5–14°S), but low at the narrow shelf area south of 15°S and in partly above the shallow shelf between 10°S and 14°S (sulphidic conditions) following previous observations and model studies (Bruland et al., 2005; Franz et al., 2012; Scholz et al., 2014; Messié and Chavez, 2014). Accordingly, we can distinguish between the HNLC areas (offshore and North) and the high PP shelf areas, which can be further divided into: regime I – 5–10°S, moderate upwelling of nutrients and high Fe supply from the wide shelf; regime II – 10–14°S, strong upwelling and PP, high Fe from the wide shelf, but potentially affected by sulphidic conditions; regime III – 15°S, strong upwelling but low Fe supply from the narrow shelf.

The subdivision into HNLC, regime I, II and III is clearly reflected by the distribution of surface sediment $bSiO_2$ values and Si:C ratios, with <10% $bSiO_2$ and Si:C = 1 in regime I, >10% $bSiO_2$ and variable Si:C of 1–3 in regime II and 15–20% $bSiO_2$ and Si:C = 3 in regime III. Based on this subdivision we will discuss the implications of the distribution of the different proxies within the surface sediment in the following sections.

4.1.1. Relationship between $\delta^{30}Si_{bSiO2}$ and $\delta^{30}Si_{Coscino}$ in core-top sediments

The HNLC condition in the northern area should be reflected by relatively high $Si(OH)_4$ utilisation and consequently high $\delta^{30}Si$ values, but only $\delta^{30}Si_{Coscino}$ signatures are observed to be high (mean: +1.6‰) while $\delta^{30}Si_{bSiO2}$ are low (mean: +0.6‰) (Fig. 1d). Towards the South along the shelf the $\delta^{30}Si_{Coscino}$ signatures remain high while the $\delta^{30}Si_{bSiO2}$ signatures increase from +0.7‰ to +1.1‰. Consequently, the $\Delta^{30}Si_{coscino-bSiO2}$ values decrease from 0.7‰ to 0.3‰ (averaged values; Fig. 1d; Table 1), which suggests increased Si utilisation concomitant with an intensification of upwelling conditions. However, with increasing upwelling intensity one would generally expect lower $\delta^{30}Si_{bSiO2}$ values and less complete Si utilisation in the southern part of the upwelling area, due to the continuous re-supply of unfractionated subsurface nutrients to surface waters. Conversely, $\delta^{30}Si_{Coscino}$ signatures show little variations and are all close to +1.5‰, reflecting near-complete Si utilisation (i.e. the diatom isotopic composition is close to that of the subsurface water/PCUC or source water value of +1.5‰ assuming steady-state/open system conditions; Fig. 1d; Table 1). In agreement with Ehlert et al. (2012), we suggest that the seasonal changes and succession of the diatom assemblages may have a major influence on the $\delta^{30}Si_{bSiO2}$ values.

Comparison of our $\delta^{30}Si$ signatures and $\Delta^{30}Si_{coscino-bSiO2}$ values with previously reported surface sediment diatom assemblages (Schuette, 1980) shows that the near-shore area between 10°S and 15°S, where high $\delta^{30}Si_{bSiO2}$ (up to +1.1‰) prevail, is dominated by Chaetoceros RS and T. nitzschioides (upwelling-related species), associated with low abundances of non-upwelling species. In contrast, between 5°S and 10°S, further away from the coast, moderate $\delta^{30}Si_{bSiO2}$ values (+0.7‰) are linked to increased percentages of non-upwelling species over upwelling-related species. Thus, the southward decrease in $\Delta^{30}Si_{coscino-bSiO2}$ coincides with a shift in diatom assemblages from low percentages of upwelling-related diatoms (regime I = high $\Delta^{30}Si_{coscino-bSiO2}$), via moderate percentages (regime II = moderate $\Delta^{30}Si_{coscino-bSiO2}$), to high percentages of upwelling-related diatoms associated with decreased contribution of non-upwelling diatoms (regime III = low $\Delta^{30}Si_{coscino-bSiO2}$). Changes in hydrography can lead to significant seasonal variations of both dissolved $\delta^{30}Si_{Si(OH)4}$ and particulate $\delta^{30}Si_{bSiO2}$ signatures, as observed for example in the South China Sea (Cao et al., 2012). Thus, the changes in $\Delta^{30}Si_{coscino-bSiO2}$ concomitant with a shift in the diatom assemblage are likely caused by seasonality and environmental conditions (i.e. upwelling strength, nutrient availability) within the three regimes (I, II and III). To better understand this linkage we will have a more detailed look at the seasonal diatom succession stages under present-day upwelling and non-upwelling conditions in the following section.

4.1.2. The seasonal effect on diatom assemblages and consequences for the $\delta^{30}Si$ signal

During seasonally weaker upwelling of nutrients, upwelling-related diatom species are reduced to low contri-

butions of *T. nitzschioides* and *Chaetoceros* spp. (Rojas de Mendiola, 1981), whereas coastal planktonic species dominate, reflecting non-upwelling (more stratified) conditions and an advanced succession stage. In contrast, the enhanced upwelling of nutrients during spring and fall causes intense blooms of *Chaetoceros* spp., *S. costatum* or *T. nitzschioides* (Rojas de Mendiola, 1981), small opportunistic diatom species (i.e. upwelling-related diatoms). However, following the initial bloom of upwelling-related diatoms relaxation phases between upwelling events cause continuous nutrient consumption and coastal planktonic diatom species, as well as the formation of resting spores (RS) emerge, even under seasonally strong upwelling conditions. Overall, aged surface waters depleted in nutrients favour large centric diatom species (coastal planktonic species; *Coscinodiscus* spp.) with low growth rates. As these large centric diatoms represent a later succession stage in the evolution of blooms and already more stratified waters (Tarazona et al., 2003) they are representative of weaker upwelling, higher nutrient utilisation and thus reveal higher $\delta^{30}Si$ values.

The question arises if and how the $\delta^{30}Si_{bSiO2}$ surface sediment record reflects these seasonal differences in PP upwelling intensity and diatom assemblages. The water column $\delta^{30}Si_{Si(OH)4}$ during summer presented by Ehlert et al. (2012) indicated high PP but low $Si(OH)_4$ utilisation between 10°S and 15°S, where active upwelling and re-supply of nutrients occurred. However, the corresponding $\delta^{30}Si_{bSiO2}$ in surface sediments from this area are highest (+1.1‰) indicating higher than the observed Si utilisation in the present-day water column. Therefore, either the available water column data only reflect a snapshot of the seasonal upwelling variability and $\delta^{30}Si_{bSiO2}$ signatures may increase further with proceeding diatom productivity, or the $\delta^{30}Si_{bSiO2}$ is biased by the diatom assemblage within the 11–32 µm fraction. *T. nitzschioides* and *Chaetoceros* spp. (and *S. costatum*) are preferentially removed from the samples measured for $\delta^{30}Si_{bSiO2}$ during sample preparation (see Sections 2.2 and 3.2). Hence, the 11–32 µm fraction mainly consists of *Chaetoceros* RS and small coastal planktonic diatoms (Supplementary Material, Fig. S3). The resulting $\delta^{30}Si_{bSiO2}$ signatures may lack a significant part of the diatom assemblage containing low isotopic values belonging to the early succession stage (initial upwelling) and rather reflect higher $\delta^{30}Si_{bSiO2}$ signatures from small coastal planktonic species included in more advanced stages of the succession (Fig. 3b and c). Furthermore, the formation of RS with progressive nutrient depletion, which should hence record higher $\delta^{30}Si_{bSiO2}$ values, and subsequent re-seeding by upwelling, could also increase the initial $\delta^{30}Si_{bSiO2}$ signal. Overall, this strong upwelling scenario best explains the conditions at 10–15°S (regime II and III; Fig 3b and c), which is characterised by most intense upwelling conditions consistent with the observed diatom assemblages in the underlying sediments.

In contrast, at the wide shelf area between 5°S and 10°S, moderate mean $\delta^{30}Si_{bSiO2}$ values (+0.7‰) relate to increased percentages of non-upwelling diatom species and reduced contribution of upwelling-related species. As these samples are outside the influence of near-shore coastal upwelling and thus do not comprise intense blooms of upwelling-related species, they should reflect overall weaker upwelling or summer conditions. Low contributions of *Chaetoceros* spp. and *T. nitzschioides* mark a minor initial diatom succession/bloom prior to the appearance of small coastal planktonic diatoms. Thus, nutrient utilisation and Si isotope fractionation are lower when these small coastal planktonic diatoms bloom. This results in the observed lower $\delta^{30}Si_{bSiO2}$ values of the small diatom fraction in comparison to upwelling induced blooms and in a higher difference ($\Delta^{30}Si_{coscino-bSiO2}$) between small and large centric (coastal) diatoms (Fig. 3a).

Accordingly, we propose that (1) the $\delta^{30}Si_{bSiO2}$ values are highest between 10°S and 15°S because the upwelling of nutrient-rich waters results in more pronounced blooming events and re-seeding of RS (low $\Delta^{30}Si_{coscino-bSiO2}$; regime II and III); (2) where weak upwelling prevails (seasonal or regional) $\delta^{30}Si_{bSiO2}$ values are lower because the lack of intense bloom events lowers the Si fractionation of the small diatom fraction (high $\Delta^{30}Si_{coscino-bSiO2}$; regime I); (3) the $\delta^{30}Si_{Coscino}$ signatures record high Si utilisation either during summer or under stratified conditions of the advanced succession stage of upwelling blooms. Unfortunately, there are to date no further seasonally resolved dissolved $\delta^{30}Si_{Si(OH)4}$ or diatom ($\delta^{30}Si_{Coscino}$ and $\delta^{30}Si_{bSiO2}$) data allowing the investigation of an entire production cycle to test the hypothetical scenarios 1, 2 and 3 described above.

Nevertheless, to reconstruct past conditions off Peru we will apply the observed three scenarios (1, 2 and 3, respectively) for determining upwelling strength and nutrient availability from the downcore record at 15°S, covering the last 17,700 years in the following section. Although the observed relationship of strong upwelling and high nutrient supply with highest $\delta^{30}Si_{bSiO2}$ values that indicate high utilisation is generally counterintuitive a similar relationship has been reported previously in the Gulf of California Coastal Upwelling system (GoC; Pichevin et al., 2014). In contrast to the Peruvian Coastal Upwelling system upwelling conditions and relaxation in the GoC show a strong seasonality, and large diatoms such as *Coscinodiscus* spp. are reported to adapt to more stratified condition by thriving in a deep chlorophyll maximum. Although such conditions should also lead to high Si utilisation and high $\delta^{30}Si_{Coscino}$ values isotopic signatures will ultimately be influenced by the source water signatures ($\delta^{30}Si_{SiOH4}$). Therefore, we suggest that $\Delta^{30}Si_{coscino-bSiO2}$ values in other regions may differ from our observation. However as long as $\delta^{30}Si_{bSiO2}$ mirrors upwelling conditions and $\delta^{30}Si_{Coscino}$ relaxation as well as near complete $Si(OH)_4$ utilisation, $\Delta^{30}Si_{coscino-bSiO2}$ values should still reflect variations in upwelling conditions.

4.1.3. Effects of upwelling intensity and nutrient limitation on the surface sediment $\delta^{30}Si_{bSiO2}$ record

The availability of nutrients in the surface waters regulates PP ultimately influencing nutrient utilisation and the diatom species assemblages. NO_3^- or PO_4 limitation is generally not observed off Peru, instead $Si(OH)_4$ limitation has been widely suggested to limit PP off Peru (Dugdale et al.,

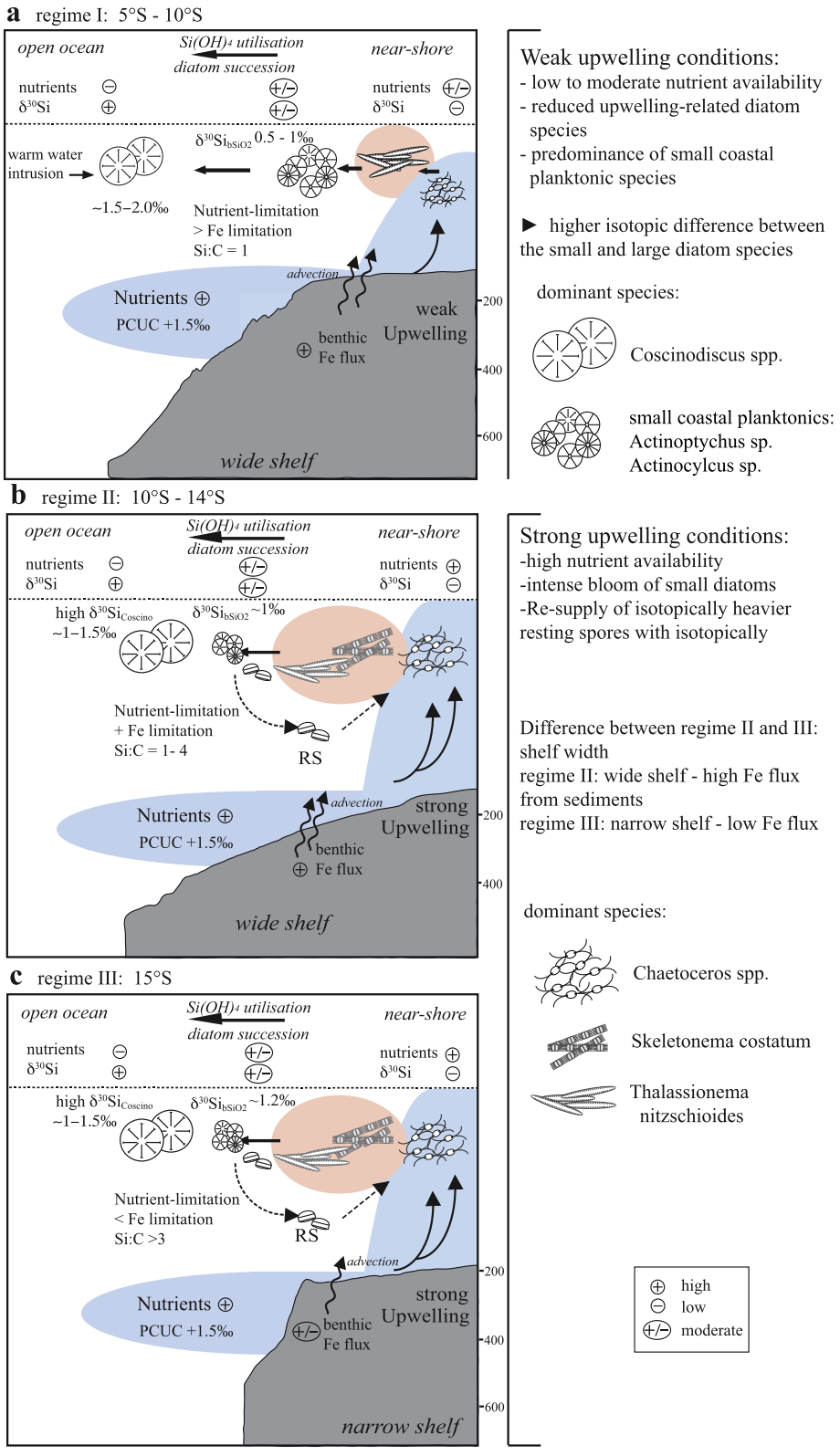

Fig. 3. Schematic model showing seasonal or interannual diatom productivity for: (a) regime I (5–10°S): weak upwelling conditions nutrient > iron limitation; (b) regime II (10–14°S): strong upwelling conditions with nutrient > iron limitation; (c) regime III (15°S): strong upwelling conditions with iron > nutrient limitation.

2002; Franz et al., 2012). A possible mechanism that leads to preferential $Si(OH)_4$ uptake over NO_3^- (and carbon (C)) is Fe limitation leading to increased Si:N (and Si:C) ratios (Hutchins and Bruland, 1998; Takeda, 1998; De La Rocha et al., 2000; Hutchins et al., 2002; Sarthou et al., 2005). Thus, under Fe deficient conditions diatoms increase frustule thickness leading to higher gravitational export but decrease the internal organic matter content. However, species effects can also lead to less silicified and organic-rich diatom frustules.

The reduced Fe availability concomitant with intense upwelling conditions support the observations of Pichevin et al. (2014) that with ongoing PP and nutrient consumption during upwelling blooms Fe becomes limiting leading to a high uptake of Si relative to NO_3^- and carbon thereby enhancing the Si burial due to frustule thickening. Accordingly, global Si:C ratios of settling particles between 1 and 10 are found in areas of high Si fluxes (Southern Ocean, North Pacific and equatorial Pacific; Pichevin et al., 2014). Therefore, we conclude that the high Si:C ratios in the surface sediments of Northern Peru and at the southern shelf close to the coast between 10°S and 15°S indicate iron limitation in these areas. However, while the HNLC is generally characterised by co-limitation of Si and Fe, the shelf area indicates transient Fe deficiency during enhanced upwelling. This means that initial macro- and micronutrient conditions are ideal for diatom blooms, but with on-going nutrient consumption Fe stress leads to frustule thickness and high Si:C ratios. This observation adds to our conclusions that $\delta^{30}Si_{bSiO2}$ signatures are higher where upwelling is most intense. Accordingly, the high $\delta^{30}Si_{bSiO2}$ values observed in regime II and III could in part be induced by the transient Fe limitation increasing the $Si(OH)_4$ utilisation via frustule thickening towards the end of upwelling blooms. However, so far a detailed study comparing nutrient ratios in surface waters with that of particulate organic matter is lacking off Peru. Therefore, we suggest that Fe stress might influence $\delta^{30}Si_{bSiO2}$ but is not the major mechanism to explain our observations.

4.2. Reconstruction of past conditions

4.2.1. Combining silicic acid utilisation and diatom assemblages

As shown above the present-day shelf region off Peru is characterized by variations in the timing and duration of blooming events induced by the upwelling of nutrient-rich waters. We now want to apply the changes in diatom assemblages and Si isotope compositions, which are directly related to these different environmental conditions to reconstruct nutrient utilisation and upwelling intensity on longer timescales. We find that downcore AR_{bSiO2}, Si:C ratios, $\delta^{30}Si_{bSiO2}$ and $\delta^{30}Si_{Coscino}$ isotope data as well as diatom assemblages exhibit a pronounced shift between the deglaciation and the Holocene and that the isotopic offset ($\Delta^{30}Si_{coscino-bSiO2}$) has been a persistent feature off Peru, at least during the past 17,700 years (Table 2).

During the deglaciation the low AR_{bSiO2} and total diatom abundances reflect decreased PP. According to low $\delta^{30}Si_{bSiO2}$ and Si:C this indicates enhanced Fe deficiency with concomitant reduced Si utilisation. Similar low $\delta^{30}Si_{bSiO2}$ values were also measured in core SO147-106KL from 12°S (Fig. 2d; Ehlert et al., 2013). The diatom assemblages from our core 003–2 indicate a modest contribution of upwelling-related diatoms (mean: $50 \pm 20\%$), while relative abundances of coastal planktonic (non-upwelling species) are elevated (mean: $20 \pm 10\%$; Fig. 2a and b), further confirming diminished upwelling intensity. Hence, weaker upwelling likely caused low diatom PP due to decreased nutrient supply to the photic zone, similar to present-day conditions between 5°S and 10°S. This is confirmed by high $\Delta^{30}Si_{coscino-bSiO2}$ values of $+0.8 \pm 0.1$‰ close to the offset reported for regime I ($\Delta^{30}Si_{coscino-bSiO2} = 0.8$‰). However, the deglacial $\delta_{30}Si_{Coscino}$ signatures remained considerably lower than modern values at +1.1‰, although Si:C are increased indicating Fe limitation. As observed within modern surface sediments when iron is limiting either PP is low associated with low $\delta^{30}Si_{bSiO2}$ and high $\delta^{30}Si_{Coscino}$ values (HNLC area), or PP is intense with high $\delta^{30}Si_{bSiO2}$ and prolonged Fe limitation associated with coastal upwelling blooms. The only available record for past Fe export so far indicates a trend from high to low excess Fe from shelf sediments from the last glacial (21 ka BP) towards the end of the deglaciation (~12 ka BP; Scholz et al., 2014). The simultaneously low $\delta^{30}Si_{Coscino}$ values which should increase under conditions of both Fe limitation and low silicate availability indicate either a change towards an isotopically lighter signal from the source waters, or a limitation of nutrients other than $Si(OH)_4$, such as NO_3^-, causing less complete $Si(OH)_4$ utilisation of source waters. The latter is supported by increased $\delta^{15}N$ values reported for the deglaciation off Peru due to increased denitrification under less oxygenated conditions, as well as more complete NO_3^- utilisation (Higginson, 2004; Scholz et al., 2014). Furthermore, RS formation of *Chaetoceros* spp. seems to be especially linked to NO_3^- limitation (Garrison, 1981; Oku and Kamatani, 1997). Thus, the high abundance of RS during the deglaciation could have been promoted by NO_3^- limitation.

At the transition from the deglaciation to the Early Holocene (11–8 ka BP) higher AR_{bSiO2} values and total diatom abundance are linked to a marked increase in the relative abundance of upwelling-related diatom species indicating greater upwelling intensity compared to the deglaciation. Interestingly, the $\delta^{30}Si_{bSiO2}$ record remained stable at moderate values (+0.8‰) while the $\delta^{30}Si_{Coscino}$ signature increased to +1.4‰, resulting in $\Delta^{30}Si_{coscino-bSiO2}$ values >0.6‰. In contrast, the record of SO147-106KL shows higher variability and shifts between high (+1.1‰) and low (+0.4‰) $\delta^{30}Si_{bSiO2}$ values (Fig. 2d). Thus, core 003-2 generally demonstrates a shift towards stronger upwelling conditions (regime II), but most likely the pronounced upwelling intensification at 10 ka BP is missing in the $\delta^{30}Si_{bSiO2}$ record as no sample was taken exactly for this time. In contrast, core SO147-106KL further to the North shows high variability with shifts between conditions of weakened (regime I) and periodically higher upwelling intensity and Si utilisation (regime II). These highly

dynamic changes may have been induced by alternation of enhanced La Niña and El Niño-like conditions (Ehlert et al., 2013).

During the Mid to Late Holocene the variability of $\delta^{30}Si$, AR_{Corg} and diatom abundances are higher, reflecting periods of enhanced PP and $Si(OH)_4$ utilisation. This is especially true for three periods of enhanced AR_{Corg} values at 8.2–7.9 ka and 5.2–4.1 ka BP with peak values of Si:C and $\delta^{30}Si_{bSiO2}$. Simultaneously, the amount of *Chaetoceros* (RS) shows a marked decrease, while *S. costatum* often dominated the diatom assemblage (Fig. 2b). Such a dominance of *S. costatum* over *Chaetoceros* spp. within the diatom assemblage is commonly observed today at our study site during fall (Rojas de Mendiola, 1981) indicating a shift to intensified fall diatom blooms. This *S. costatum* dominance is linked to low $\Delta^{30}Si_{coscino-bSiO2}$ values (<0.3‰), thus supporting strong upwelling conditions and intense PP (regime III). In between the peak PP values, AR_{Corg} and diatom abundances indicate reduced PP in combination with weaker upwelling as shown by lower $\delta^{30}Si_{bSiO2}$ (+0.8‰) and higher $\Delta^{30}Si_{coscino-bSiO2}$ values (+0.3‰ to +0.6‰). Thus, the Holocene was characterised by generally intensified upwelling conditions in comparison to the deglaciation at our core location, Mid to Late Holocene conditions varied between moderate and high nutrient concentrations similar to those measured in the present-day centre of the upwelling area (regimes II and III; 10–15°S).

Overall the shift we observe in the $\delta^{30}Si_{bSiO2}$ and $\delta^{30}Si_{Cosino}$ records between the deglaciation and the Holocene highlights the transition from low to intensified Si $(OH)_4$ utilisation, as well as the intensification of upwelling conditions. This shift was associated with diatom assemblages that reflect a short upwelling season (deglaciation) to an assemblage indicative of a prolonged blooming season and more intense upwelling (Holocene). Thus, our findings from core-top sediments, showing that a smaller $\Delta^{30}Si_{coscino-bSiO2}$ is associated with more intense upwelling and stronger Si utilisation as well as Fe limitation can be applied to the paleo record. Accordingly, the observed switch from high $\Delta^{30}Si_{coscino-bSiO2}$ during the deglaciation to low $\Delta^{30}Si_{coscino-bSiO2}$ values during the Holocene is consistent with a shift from weak to enhanced upwelling conditions.

4.3. The influence of varying diatom assemblages on the $\delta^{30}Si$ record

Environmental conditions, such as upwelling intensity and nutrient availability, alter the amount of Si utilisation and thus the Si isotope composition of diatoms by regulating the diatom succession, the duration of blooming events, and the initiation of nutrient depletion. However, a bias on the Si isotope composition in biogenic silica may arise by the species-specific Si isotope fractionation factors of different diatom species. A crucial assumption for the paleo reconstructions of nutrient utilisation and PP based on $\delta^{30}Si$ has so far been that the isotopic enrichment factor during the incorporation of silicon in diatoms is species independent (De La Rocha et al., 1997). The recent study by Sutton et al. (2013) suggested species-dependent fractionation factors between −0.5‰ and −2.1‰, thus highlighting that changes in diatom assemblages could cause significant variability in $\delta^{30}Si$ records without changes in nutrient utilisation. Therefore, we will follow the approach of Sutton et al. (2013) and estimate the influence of the taxonomic composition on past $\delta^{30}Si$ records that considers the relative diatom species abundance as well as their specific isotope enrichment factor $^{30}\varepsilon$.

So far mainly polar or sub-polar diatom species have been studied regarding their fractionation factors, but isotope fractionation factors obtained from culturing studies can be found for *Chaetoceros brevis*, *S. costatum* and for various subgenera of Thalassiosira, roughly matching the species prevailing off Peru (De La Rocha et al., 1997; Sutton et al., 2013). Although, the $^{30}\varepsilon$ factors reported for *S. costatum* and *Thalassiosira* sp. range from −0.4 to −1.2‰ and from −0.4 to −1.8‰, respectively, the corresponding mean values of −1.1‰ are similar to the mean enrichment factor previously assumed for all diatom species (De La Rocha et al., 1997). Only for Chaetoceros brevis a significantly larger enrichment factor of $^{30}\varepsilon = -2.09‰$ was reported. Thus, we test the potential influence of the different enrichment factors on our downcore record of core 003-2 by applying the model calculation adapted from Sutton et al. (2013). To calculate the variability in $^{30}\varepsilon$ caused by changes in the diatom assemblage (ε_{ass}, hereafter), we used the following equation:

$$\varepsilon_{ass} = (C/100 \times (-2.09‰)) + (O/100 \times (-1.1‰)) \quad (1)$$

where C and O are the abundances of *Chaetoceros* spp. (RS) and other diatom species, respectively (Table 3, columns 3 and 4). For Chaetoceros spp. we applied a $^{30}\varepsilon$ value of −2.09‰ from Chaetoceros brevis (Sutton et al., 2013) and −1.1‰ (De La Rocha et al., 1997) was used as a mean value for the other diatom species. Like Sutton et al. (2013) we assume that the *Chaetoceros* spp. (RS) have the same enrichment factor as vegetative cells due to the lack of isotopic measurements of the RS themselves. So far little is known what controls the Si isotope fractionation within diatoms, but growth and uptake rates are generally associated with $Si(OH)_4$ availability (Sarthou et al., 2005). Thus, Hendry et al. (2010) speculated that, based on a similar observation for sponge spicule formation, if the fractionation process occurs at the site of Si uptake a higher uptake rate may lead to higher fractionation. Although RS are formed under nutrient deplete conditions growth rates are reported to be similar to those of the vegetative cells (Oku and Kamatani, 1997), potentially resulting in a similar isotope fractionation.

Based on Eq. (1) ε_{ass} will have values between −1.1‰ and −2.09‰. High values close to −1.1‰ relate to low amounts of RS and ε_{ass} will decrease towards −2.09‰ when RS amounts increase. The calculated ε_{ass} values range between −1.27‰ and −1.84‰ for the entire core (Table 3, column 6). To assess the effect on the $\delta^{30}Si_{bSiO2}$ signature in the core we applied the calculated ε_{ass} using following equation (Fry, 2006; Sutton et al., 2013):

$$\delta^{30}Si_{\varepsilon ass} = \delta^{30}Si_{Si(OH)4source} + {}^{30}\varepsilon_{ass} \quad (2)$$

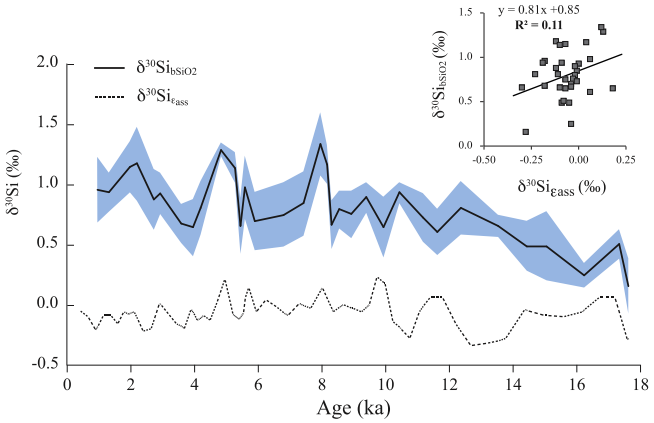

Fig. 4. Comparison of $\delta^{30}Si_{bSiO2}$ (‰) record (thin black line with uncertainties indicated by blue shaded area) with model estimations for $\delta^{30}Si_{\varepsilon ass}$ (black dotted line). Left: steady state model assumptions with ε_{ass} based on *Chaetoceros* RS abundance (black thick line). Right: $\delta^{30}Si_{\varepsilon ass}$ versus $\delta^{30}Si_{bSiO2}$ ($R^2 = 0.11$, negative correlation). (For interpretation of the references to colour in this figure legend, the reader is referred to the web version of this article.)

where $\delta^{30}Si_{\varepsilon ass}$ is the isotopic composition of accumulated biogenic silica (mixed small diatoms) and $\delta^{30}Si_{Si(OH)4source}$ reflects the source water. The $\delta^{30}Si_{Si(OH)4source}$ was set to +1.5‰, ($\delta^{30}Si_{SiOH4}$ of the PCUC; Ehlert et al., 2012). In contrast to Sutton et al. (2013) we did not use a mixed layer value for $\delta^{30}Si_{Si(OH)4source}$, as we want to evaluate the potential species-specific effect independent from any influence of utilisation (the mean $\delta^{30}Si_{Si(OH)4}$ mixed layer value would be +2‰). Obviously by neglecting the amount of utilisation the estimated $\delta^{30}Si_{\varepsilon ass}$ signatures are lower than the equivalent $\delta^{30}Si_{bSiO2}$ values.

The resulting values for $\delta^{30}Si_{\varepsilon ass}$ are shown in comparison to measured $\delta^{30}Si_{bSiO2}$ values (Fig. 4). These results show that the amount of RS cannot explain the high variability observed in the measured $\delta^{30}Si_{bSiO2}$ record, as there is essentially no correlation between modelled $\delta^{30}Si_{\varepsilon ass}$ and measured $\delta^{30}Si_{bSiO2}$ ($R^2 = 0.11$). As we only included the specific $^{30}\varepsilon$ for *Chaetoceros brevis* (for *S. costatum* and *Thalassiosira* sp. mean value is = −1.1‰ included in *O*, respectively; De La Rocha et al., 1997) in our calculation, the knowledge of additional enrichment factors of other diatom species may help to deconvolve the effect of species composition observed in this study. It would be especially interesting to see if growth rates and $Si(OH)_4$ availability control the isotope fractionation, as the observed high $\delta^{30}Si_{bSiO2}$ values associated with high growth rates and $Si(OH)_4$ concentrations during intense upwelling could be further influenced by higher isotope fractionation. The minor impact of a species-dependent fractionation on $\delta^{30}Si_{bSiO2}$ suggests that the variability of $Si(OH)_4$ utilisation in the surface waters controlled by environmental changes, has the strongest effect on both the dissolved and particulate $\delta^{30}Si$ signal.

5. CONCLUSIONS

In this study we combine for the first time surface sediment mixed-species $\delta^{30}Si_{bSiO2}$ and mono-generic $\delta^{30}Si_{Coscino}$ (i.e. *Coscinodiscus* spp.) signatures with diatom assemblages to determine present and past silicate utilisation and upwelling intensity in the Peruvian upwelling region. We find a pronounced environmental control by upwelling intensity and nutrient availability on all applied proxies. Changes in the abundance of upwelling-related diatom species versus non-upwelling diatom species reflect the strength of nearshore upwelling, whereas $\delta^{30}Si_{bSiO2}$ signatures represented the small diatom fraction change in relation to Si utilisation, iron limitation and diatom succession stages.

Based on our results the modern Peruvian shelf can be subdivided into distinct regimes: Regime II and III denote strong upwelling reflected by intense blooms of small rapidly growing diatom species followed by the production of larger centric diatoms and the formation of resting spores (RS) as nutrient and iron depletion in surface waters proceeds. Due to the fractional loss of the smaller diatoms, the measured 11–32 μm fraction ($\delta^{30}Si_{bSiO2}$) lacks the initial diatom succession stage but concentrates isotopically heavier small coastal planktonic diatom species as well as RS, resulting in overall high $\delta^{30}Si_{bSiO2}$ values (+1.1‰) and a low offset between $\delta^{30}Si_{Coscino}$ and $\delta^{30}Si_{bSiO2}$ ($\Delta^{30}Si_{coscino-bSiO2}$). In contrast regime I is characterised by weak upwelling conditions and by moderate nutrient and high iron availability accompanied by prolonged surface water stratification. This results in reduced contributions of upwelling-related diatom species but promote the dominance of coastal planktonic diatom species. After the initial diatom succession stage and intense blooming events are terminated, Si utilisation and isotope fractionation remain low until small coastal planktonic diatoms record the lower $\delta^{30}Si_{bSiO2}$ signal resulting in a higher $\Delta^{30}Si_{coscino-bSiO2}$.

Downcore reconstructions of Core M77/2-003-2 show for the first time a persistent offset ($\Delta^{30}Si_{coscino-bSiO2}$) combined with a marked shift from weak Deglacial to strong Holocene upwelling conditions. The comparison of the Si isotopic compositions with the reported diatom assemblage shows that the major shift in past $\Delta^{30}Si_{coscino-bSiO2}$ values was linked to an increase of upwelling-related diatom species during the Holocene. Consequently, variations in the past upwelling intensity and nutrient availability have been closely linked with the different regimes (I, II and III) observed today within the Peruvian upwelling area.

We conclude that during the vast interannual and seasonal changes in the intensity of upwelling off Peru, the degree of silicate utilisation and the associated diatom assemblages have exerted the most important control on the δ^{30}Si record of the diatoms, whereas variable isotope enrichment factors of different diatom species have only had minor influence. Consequently, the combined use of diatom assemblages and δ^{30}Si signatures of different size fractions allows the reliable reconstruction of past silicate utilisation and upwelling intensity. Further improvements can be achieved by extended seasonal information from the present day water column given that the $\delta^{30}Si_{bSiO2}$ may be biased by the fractional loss of important species.

ACKNOWLEDGEMENTS

This work is a contribution of the Collaborative Research Project 754 "Climate-Biogeochemistry interactions in the Tropical Ocean" (www.sfb754.de), which is supported by the Deutsche Forschungsgemeinschaft (DFG, German Research Foundation).

APPENDIX A. SUPPLEMENTARY DATA

Supplementary data associated with this article can be found, in the online version, at http://dx.doi.org/10.1016/j.gca.2015.12.029.

REFERENCES

Abrantes F., Lopes C., Mix A. and Pisias N. (2007) Diatoms in Southeast Pacific surface sediments reflect environmental properties. *Quatern. Sci. Rev.* **26**, 155–169.

Albarède F., Telouk P., Blichert-Toft J., Boyet M., Agranier A. and Nelson B. (2004) Precise and accurate isotopic measurements using multiple-collector ICPMS. *Geochim. Cosmochim. Acta* **68**, 2725–2744.

Ayón P., Criales-Hernandez M. I., Schwamborn R. and Hirche H.-J. (2008) Zooplankton research off Peru: a review. *Prog. Oceanogr.* **79**, 238–255.

Barber R. T. and Chávez F. P. (1991) Regulation of primary productivity rate in the equatorial Pacific. *Limnol. Oceangr.* **36**, 1803–1815.

Beucher C. P., Brzezinski M. A. and Crosta X. (2007) Silicic acid dynamics in the glacial sub-Antarctic: implications for the silicic acid leakage hypothesis. *Global Biogeochem. Cycles* **21**, 3015–3028.

Beucher C. P., Brzezinski M. A. and Jones J. L. (2008) Sources and biological fractionation of Silicon isotopes in the Eastern Equatorial Pacific. *Geochim. Cosmochim. Acta* **72**, 3063–3073.

Blaauw M. (2010) Quaternary geochronology. *Quat. Geochronol.* **5**, 512–518.

Blasco D. (1971) Compsición y distribución del fitoplancton en la región del afliamientio de las costas peruanas. *Inv. Pesq.*, 61–112.

Blasco D., Estrada M. and Jones B. H. (1981) Short time variability of phytoplankton populations in upwelling regions—the example of northwest Africa. *Coastal Estuarine Sci.* **1**, 339–347.

Brink K. H., Halpern D., Huyer A. and Smith R. L. (1983) The physical-environment of the Peruvian upwelling system. *Prog. Oceanogr.* **12**, 285–305.

Bruland K. W., Rue E. L., Smith G. J. and DiTullio G. R. (2005) Iron, macronutrients and diatom blooms in the Peru upwelling regime: brown and blue waters of Peru. *Mar. Chem.* **93**, 81–103.

Cao Z., Frank M., Dai M., Grasse P. and Ehlert C. (2012) Silicon isotope constraints on sources and utilization of silicic acid in the northern South China Sea. *Geochim. Cosmochim. Acta* **97**, 88–104.

Cardinal D., Alleman L. Y., Dehairs F., Savoye N., Trull T. W. and André L. (2005) Relevance of silicon isotopes to Si-nutrient utilization and Si-source assessment in Antarctic waters. *Global Biogeochem. Cycles* **19**, GB2007.

Cardinal D., Savoye N., Trull T. W., Dehairs F., Kopczynska E. E., Fripiat F., Tison J.-L. and André L. (2007) Silicon isotopes in spring Southern Ocean diatoms: large zonal changes despite homogeneity among size fractions. *Mar. Chem.* **106**, 46–62.

Crosta X. and Koç N. (2007) Diatoms: from micropaleontology to isotope geochemistry. In *Proxies in Late Cenozoic Paleoceanography, Developments in Marine Geology*, vol. 1 (eds. C. Hilaire-Marcel and A. de Vernal). Elsevier, Amsterdam, The Netherlands, pp. 327–369.

Czeschel R., Stramma L., Schwarzkopf F. U., Giese B. S., Funk A. and Karstensen J. (2011) Middepth circulation of the eastern tropical South Pacific and its link to the oxygen minimum zone. *J. Geophys. Res.* **116**, C01015.

De La Rocha C. L., Brzezinski M. A. and DeNiro M. J. (1997) Fractionation of silicon isotopes by marine diatoms during biogenic silica formation. *Geochim. Cosmochim. Acta* **61**, 5051–5056.

De La Rocha C. L., Brzezinski M. A., DeNiro M. J. and Shemesh A. (1998) Silicon-isotope composition of diatoms as an indicator of past oceanic change. *Nature* **395**, 680–683.

De La Rocha C. L., Hutchins D. A., Brzezinski M. A. and Zhang Y. (2000) Effects of iron and zinc deficiency on elemental composition and silica production by diatoms. *Mar. Ecol. Prog. Ser.* **195**, 71–79.

de Souza G. F., Reynolds B. C., Rickli J., Frank M., Saito M. A., Gerringa L. J. A. and Bourdon B. (2012) Southern Ocean control of silicon stable isotope distribution in the deep Atlantic Ocean. *Global Biogeochem. Cycles* **26**, 2035–2047.

De Vries T. J. and Schrader H. (1981) Variation of upwelling/oceanic conditions during the latest Pleistocene through Holocene off the central Peruvian coast: a diatom record. *Mar. Micropaleontol.* **6**, 157–167.

DeMaster D. J. (1981) The supply and accumulation of silica in the marine-environment. *Geochim. Cosmochim. Acta* **45**, 1715–1732.

DiTullio G. R., Geesey M. E., Maucher J. M. and Alm M. B. (2005) Influence of iron on algal community composition and physiological status in the Peru upwelling system. *Limnol. Oceangr.* **50**, 1887–1907.

Douthitt C. B. (1982) The geochemistry of the stable isotopes of silicon. *Geochim. Cosmochim. Acta* **46**, 1449–1458.

Dugdale R. C., Wilkerson F. P. and Minas H. J. (1995) The role of a silicate pump in driving new production. *Deep-Sea Res. I* **42** (5), 697–719.

Dugdale R. C., Wischmeyer A. G., Wilkerson F. P., Barber R. T., Chai F., Jiang M. S. and Peng T. H. (2002) Meridional asymmetry of source nutrients to the equatorial Pacific upwelling ecosystem and its potential impact on ocean-atmosphere CO_2 flux: a data and modeling approach. *Deep-Sea Res II* **49**, 2513–2531.

Echevin V., Aumont O., Ledesma J. and Flores G. (2008) The seasonal cycle of surface chlorophyll in the Peruvian upwelling system: a modelling study. *Prog. Oceanogr.* **79**, 167–176.

Egan K. E., Rickaby R. E. M., Leng M. J., Hendry K. R., Hermoso M., Sloane H. J., Bostock H. and Halliday A. N. (2012) Diatom silicon isotopes as a proxy for silicic acid utilisation: a Southern Ocean core top calibration. *Geochim. Cosmochim. Acta* **96**, 174–192.

Ehlert C., Grasse P. and Frank M. (2013) Changes in silicate utilisation and upwelling intensity off Peru since the Last Glacial Maximum – insights from silicon and neodymium isotopes. *Quatern. Sci. Rev.* **72**, 18–35.

Ehlert C., Grasse P., Mollier-Vogel E., Böschen T., Franz J., de Souza G. F., Reynolds Ben C., Stramma L. and Frank M. (2012) Factors controlling the silicon isotope distribution in waters and surface sediments of the Peruvian coastal upwelling. *Geochim. Cosmochim. Acta* **99**, 128–145.

Ellwood M. J., Wille M. and Maher W. (2010) Glacial silicic acid concentrations in the Southern Ocean. *Science* **330**, 1088–1091.

Estrada M. and Blasco D. (1985). In *Phytoplankton Assemblages in Coastal Upwelling Areas* (eds. C. Bas, R. Margalef and P. Rubies). Instituto de Investigaciones Pesqueras, Barcelona.

Franz J., Krahmann G., Lavik G., Grasse P., Dittmar T. and Riebesell U. (2012) Dynamics and stoichiometry of nutrients and phytoplankton in waters influenced by the oxygen minimum zone in the eastern tropical Pacific. *Deep-Sea Res. I* **62**, 20–31.

Fripiat F., Cavagna A. J., Dehairs F., Speich S., André L. and Cardinal D. (2011) Silicon pool dynamics and biogenic silica export in the Southern Ocean inferred from Si-isotopes. *Ocean Sci.* **7**, 533–547.

Fry B. (2006) *Stable Isotope Ecology*. Springer, New York.

Fuenzalida R., Schneider W., Garcés-Vargas J., Bravo L. and Lange C. (2009) Vertical and horizontal extension of the oxygen minimum zone in the eastern South Pacific Ocean. *Deep Sea Res. II* **56**, 992–1003.

Garrison D. L. (1979) Monterey Bay phytoplankton I. Seasonal cycles of phytoplankton assemblages. *J. Plankton Res.* **1**, 241–265.

Garrison D. L. (1981) Monterey Bay phytoplankton. II. Resting spore cycles in coastal diatom populations. *J. Plankton Res.* **3**, 137–156.

Georg R. B., Reynolds B. C., Frank M. and Halliday A. N. (2006) New sample preparation techniques for the determination of Si isotopic compositions using MC-ICPMS. *Chem. Geol.* **235**, 95–104.

Grasshoff K., Kremling K. and Ehrhardt M. (1999) *Methods of Sewater Analysis*, 3rd ed. John Wiley & Sons.

Hansen A., Ohde T. and Wasmund N. (2014) Succession of micro- and nanoplankton groups in aging upwelled waters off Namibia. *J. Mar. Syst.* **140**, 130–137.

Hendry K. R., Georg R. B., Rickaby R. E. M., Robinson L. F. and Halliday A. N. (2010) Deep ocean nutrients during the Last Glacial Maximum deduced from sponge silicon isotopic compositions. *Earth Planet. Sci. Lett.* **292**, 290–300.

Higginson M. J. (2004) Initial test of the silicic acid leakage hypothesis using sedimentary biomarkers. *Geophys. Res. Lett.* **31**, L18303.

Hutchins D. A. and Bruland K. W. (1998) Iron-limited diatom growth and Si:N uptake ratios in a coastal upwelling regime. *Nature* **393**, 561–564.

Hutchins D. A., Hare C. E., Weaver R. S., Zhang Y., Firme G. F., DiTullio G. R., Alm M. B., Riseman S. F., Maucher J. M., Geesey M. E., Trick C. G., Smith G. J., Rue E. L., Conn J. and Bruland K. W. (2002) Phytoplankton iron limitation in the Humboldt Current and Peru Upwelling. *Limnol. Oceangr.* **47**, 997–1011.

Johnson K. S., Chavez F. P. and Friederich G. E. (1999) Continental-shelf sediment as a primary source of iron for coastal phytoplankton. *Nature* **398**, 1–4.

Jones B. H., Brink K. H., Dugdale R. C., Stuart D. W., Van Leer J. C., Blasco D. and Kelley J. C. (1983) Observations of a Persistent Upwelling Center off Point Conception, California. In *Coastal Upwelling Its Sediment Record*. Springer, US, Boston, MA, pp. 37–60.

Kemp A., Pike J., Pearce R. B. and Lange C. B. (2000) The "Fall dump" – a new perspective on the role of a 'shade flora' in the annual cycle of diatom production and export flux. *Deep-Sea Res. II*.

Lisitzin A. P. (1971) Ditsribution of siliceous micro fossils in suspension and in bottom sediments. In *The Micropalaeontology of Oceans* (eds. B. M. Funnell and W. R. Riedel). Cambridge Univ. Press, New York, pp. 173–195.

Lukas R. (1986) The termination of the Equatorial Undercurrent in the eastern Pacific. *Prog. Oceanogr.* **16**(2), 63–90.

MacIsaac J. J., Dugdale R. C., Barber R. T., Blasco D. and Packard T. T. (1985) Primary production cycle in an upwelling center. *Deep Sea Res. A Oceanogr. Res. Papers* **32**, 503–529.

Maier E., Chapligin B. and Abelmann A. (2013) Combined oxygen and silicon isotope analysis of diatom silica from a deglacial subarctic Pacific record. *J. Quatern. Sci.* **28**, 572–581.

Margalef R. (1978) Life-forms of phytoplankton as survival alternatives in an unstable environment. *Oceanol. Acta* **1**, 493–509.

Messié M. and Chavez F. (2014) Seasonal regulation of primary production in eastern boundary upwelling systems. *Prog. Oceanogr.* **134**, 1–18.

Mollier-Vogel E., Ryabenko E., Martinez P., Wallace D., Altabet M. A. and Schneider R. (2012) Nitrogen isotope gradients off Peru and Ecuador related to upwelling, productivity, nutrient uptake and oxygen deficiency. *Deep-Sea Res. I* **70**, 14–25.

Mollier-Vogel E. (2012) *Peruvian Oxygen Minimum Zone dynamics during the last 18,000 years* (PhD thesis). University of Kiel.

Montes I., Colas F., Capet X. and Schneider W. (2010) On the pathways of the equatorial subsurface currents in the eastern equatorial Pacific and their contributions to the Peru–Chile Undercurrent. *J. Geophys. Res.* **115**, C09003.

Morley D. W., Leng M. J., Mackay A. W., Sloane H. J., Rioual P. and Battarbee R. W. (2004) Cleaning of lake sediment samples for diatom oxygen isotope analysis. *J. Paleolimnol.* **31**, 391–401.

Müller P. J. and Schneider R. (1993) An automated leaching method for the determination of opal in sediments and particulate matter. *Deep-Sea Res. I* **40**, 425–444.

Noffke A., Hensen C., Sommer S., Scholz F., Bohlen L., Mosch T., Graco M. and Wallmann K. (2012) Benthic iron and phosphorus fluxes across the Peruvian oxygen minimum zone. *Limnol. Oceangr.* **57**, 851–867.

Oku O. and Kamatani A. (1997) Resting spore formation of the marine planktonic diatom *Chaetoceros anastomosans* induced by high salinityand nitrogen depletion. *Mar. Biol.* **127**, 515–520.

Ortlieb L., Vargas G. and Saliège J.-F. (2011) Marine radiocarbon reservoir effect along the northern Chile–southern Peru coast (14–24°S) throughout the Holocene. *Quatern. Res.* **75**, 91–103.

Pennington J. T., Mahoney K. L., Kuwahara V. S., Kolber D. D., Calienes R. and Chavez F. P. (2006) Primary production in the eastern tropical Pacific: a review. *Prog. Oceanogr.* **69**, 285–317.

Pichevin L. E., Ganeshram R. S., Geibert W., Thunell R. and Hinton R. (2014) Silica burial enhanced by iron limitation in oceanic upwelling margins. *Nat. Geosci.* **7**, 541–546.

Pichevin L. E., Reynolds B. C., Ganeshram R. S., Cacho I., Pena L., Keefe K. and Ellam R. M. (2009) Enhanced carbon pump inferred from relaxation of nutrient limitation in the glacial ocean. *Nature* **459**, 1114–1117.

Rathburn A. E., Pichon J. J. and Ayress M. A. (1997) Microfossil and stable-isotope evidence for changes in Late Holocene palaeoproductivity and palaeoceanographic conditions in the Prydz Bay region of Antarctica. *Palaeogeogr. Palaeoclimatol. Paleaoecol.* **131**, 485–510.

Reimer P. J. and Bard E. (2013) IntCal13 and Marine13 radiocarbon age calibration curves 0–50,000 years cal BP. *Radiocarbon* **55**, 1869–1887.

Reynolds B. C., Aggarwal J., Andr L., Baxter D., Beucher C., Brzezinski M. A., Engström E., Georg R. B., Land M., Leng M. J., Opfergelt S., Rodushkin I., Sloane H. J., van den Boorn S. H. J. M., Vroon P. Z. and Cardinal D. (2007) An inter-laboratory comparison of Si isotope reference materials. *J. Anal. At. Spectrom.* **22**, 561.

Reynolds B. C., Frank M. and Halliday A. N. (2008) Evidence for a major change in silicon cycling in the subarctic North Pacific at 2.73 Ma. *Paleoceanography* **23**, PA4219.

Rojas de Mendiola B. (1981) Seasonal phytoplankton distribution along the Peruvian coast. In *Coastal upwelling Coastal and Estuarine Sciences*. American Geophysical Union, Washington, DC, pp. 348–356.

Romero O. and Hebbeln D. (2003) Biogenic silica and diatom thanatocoenosis in surface sediments below the Peru–Chile Current: controlling mechanisms and relationship with productivity of surface waters. *Mar. Micropaleontol.* **48**, 71–90.

Romero O., Mollenhauer G., Schneider R. R. and Wefer G. (2003) Oscillations of the siliceous imprint in the central Benguela Upwelling System from MIS 3 through to the early Holocene: the influence of the Southern Ocean. *J. Quat. Sci.* **18**, 733–743.

Sarthou G., Timmermans K. R., Blain S. and Tréguer P. (2005) Growth physiology and fate of diatoms in the ocean: a review. *J. Sea Res.* **53**, 25–42.

Scholz F., McManus J., Mix A. C., Hensen C. and Schneider R. R. (2014) The impact of ocean deoxygenation on iron release from continental margin sediments. *Nat. Geosci.* **7**, 433–437.

Schrader H. (1992) Coastal upwelling and atmospheric CO_2 changes over the last 400,000 years: Peru. *Mar. Geol.* **107**, 239–248.

Schrader H. J. and Gersonde R. (1978) Diatoms and silicoflagellates. *Utrecht Micropaleontol. Bull.*, 129–176.

Schuette G. (1980) *Recent Marine Diatom Taphoceoenoses off Peru and off Southwet Africa: Reflection of Coastal Upwelling*. Oregon State University.

Schuette G. and Schrader H. (1981) Diatoms in surface sediments: a reflection of coastal upwelling. *Coastal Estuarine Sci.* **1**, 372–380.

Sutton J. N., Varela D. E., Brzezinski M. A. and Beucher C. P. (2013) Species-dependent silicon isotope fractionation by marine diatoms. *Geochim. Cosmochim. Acta* **104**, 300–309.

Takeda S. (1998) Influence of iron availability on nutrient consumption ratio of diatoms in oceanic waters. *Nature* **393**, 774–777.

Tarazona J. and Arntz W. (2001) The Peruvian Coastal Upwelling System. In *Coastal Marine Ecosystems of Latin America Ecological Studies*. Springer, Berlin, Heidelberg, pp. 229–244.

Tarazona J., Gutiérrez D., Paredes C. and Indacochea A. (2003) Overview and challenges of marine biodiversity research in Peru. *Gayana* **67**, 206–231.

Toggweiler J. R., Dixon K. and Broecker W. S. (1991) The peru upwelling and the ventilation of the south-pacific thermocline. *J. Geophys. Res.* **96**, 20467–20497.

Varela D. E., Pride C. J. and Brzezinski M. A. (2004) Biological fractionation of silicon isotopes in Southern Ocean surface waters. *Global Biogeochem. Cycles* **18**, 1047–1054.

Xiong Z., Li T., Algeo T., Doering K., Frank M., Brzezinski M. A., Chang F., Opfergelt S., Crosta X., Jiang F., Wan S. and Zhai B. (2015) The silicon isotope composition of *Ethmodiscus rex* laminated diatom mats from the tropical West Pacific: implications for silicate cycling during the Last Glacial Maximum. *Palaeoceanography* **30**(7), 803–823.

Zuta S. and Guillén O. (1970) Oceanografía de las aguas costeras del Perú. *Bo. Inst. Mar. Perú* **2**, 157–324.

Associate editor: Silke Severmann